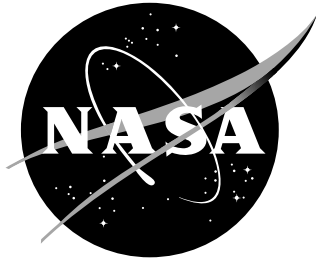


NASA/TM-1999-209552



Flight Data Reduction of Wake Velocity Measurements Using an Instrumented OV-10 Airplane

*Dan D. Vicroy, Robert A. Stuever, Eric C. Stewart, and Robert A. Rivers
Langley Research Center, Hampton, Virginia*



September 1999

The NASA STI Program Office ... in Profile

Since its founding, NASA has been dedicated to the advancement of aeronautics and space science. The NASA Scientific and Technical Information (STI) Program Office plays a key part in helping NASA maintain this important role.

The NASA STI Program Office is operated by Langley Research Center, the lead center for NASA's scientific and technical information. The NASA STI Program Office provides access to the NASA STI Database, the largest collection of aeronautical and space science STI in the world. The Program Office is also NASA's institutional mechanism for disseminating the results of its research and development activities. These results are published by NASA in the NASA STI Report Series, which includes the following report types:

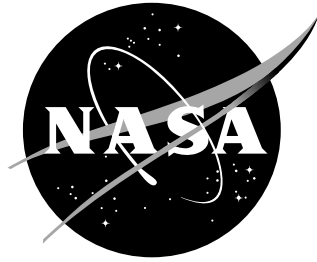
- **TECHNICAL PUBLICATION.** Reports of completed research or a major significant phase of research that present the results of NASA programs and include extensive data or theoretical analysis. Includes compilations of significant scientific and technical data and information deemed to be of continuing reference value. NASA counterpart of peer-reviewed formal professional papers, but having less stringent limitations on manuscript length and extent of graphic presentations.
- **TECHNICAL MEMORANDUM.** Scientific and technical findings that are preliminary or of specialized interest, e.g., quick release reports, working papers, and bibliographies that contain minimal annotation. Does not contain extensive analysis.
- **CONTRACTOR REPORT.** Scientific and technical findings by NASA-sponsored contractors and grantees.
- **CONFERENCE PUBLICATION.** Collected papers from scientific and technical conferences, symposia, seminars, or other meetings sponsored or co-sponsored by NASA.
- **SPECIAL PUBLICATION.** Scientific, technical, or historical information from NASA programs, projects, and missions, often concerned with subjects having substantial public interest.
- **TECHNICAL TRANSLATION.** English-language translations of foreign scientific and technical material pertinent to NASA's mission.

Specialized services that complement the STI Program Office's diverse offerings include creating custom thesauri, building customized databases, organizing and publishing research results ... even providing videos.

For more information about the NASA STI Program Office, see the following:

- Access the NASA STI Program Home Page at <http://www.sti.nasa.gov>
- E-mail your question via the Internet to help@sti.nasa.gov
- Fax your question to the NASA STI Help Desk at (301) 621-0134
- Phone the NASA STI Help Desk at (301) 621-0390
- Write to:
NASA STI Help Desk
NASA Center for AeroSpace Information
7121 Standard Drive
Hanover, MD 21076-1320

NASA/TM-1999-209552



Flight Data Reduction of Wake Velocity Measurements Using an Instrumented OV-10 Airplane

*Dan D. Vicroy, Robert A. Stuever, Eric C. Stewart, and Robert A. Rivers
Langley Research Center, Hampton, Virginia*

National Aeronautics and
Space Administration

Langley Research Center
Hampton, Virginia 23681-2199

September 1999

Available from:

NASA Center for AeroSpace Information (CASI)
7121 Standard Drive
Hanover, MD 21076-1320
(301) 621-0390

National Technical Information Service (NTIS)
5285 Port Royal Road
Springfield, VA 22161-2171
(703) **605-6000**

Contents

| | |
|---|----|
| Abstract..... | 2 |
| Introduction | 2 |
| Symbols | 2 |
| Subscripts..... | 9 |
| Superscripts..... | 9 |
| Abbreviations..... | 9 |
| Flight Test Overview..... | 10 |
| OV-10 Instrumentation | 11 |
| General System | 11 |
| Navigation Systems..... | 11 |
| Air-Data Systems | 12 |
| Airborne Video/Audio Systems..... | 13 |
| Flight Data Reduction Process..... | 13 |
| Calibration and Bias Corrections | 14 |
| Zero bias corrections | 14 |
| Rosemont 5-Hole Probe Calibration Correction..... | 15 |
| Position Error Corrections to Local Flow Angle Measurements..... | 16 |
| NACA Pitot Probe Calibration Corrections..... | 17 |
| Position Error Corrections to Static and Dynamic Pressure Measurements..... | 17 |
| Local Mach Number Calculation | 18 |
| Free-Air Temperature and Speed of Sound Calculation | 18 |
| Airplane Angular Motion Correction to Body Axis Airspeed Components | 19 |
| True Airspeed, Angle Of Attack and Sideslip Calculation..... | 19 |
| Calculation of Wind Components in Earth Axis System | 20 |
| Average Wind Speed and Direction Calculation | 21 |
| Wake Velocity Calculation..... | 21 |
| Wake Coordinate System..... | 22 |
| Wake Velocity Algorithm..... | 22 |
| Closing Remarks | 28 |
| References..... | 28 |
| Appendix A – OV-10 Airspeed Calibration..... | 47 |
| Flight Test Procedure | 47 |
| Computing Reference Values | 47 |
| Reference Angle of Attack and Sideslip Calculation..... | 47 |
| Reference Static Pressure Calculation..... | 49 |
| Compute Position Error Correction | 49 |
| Probe Static and Dynamic Pressure Calculation..... | 49 |
| Angle of Attack Calibration..... | 50 |
| Sideslip Angle Calibration..... | 51 |

Abstract

A series of flight tests to measure the wake of a Lockheed C-130 airplane and the accompanying atmospheric state have been conducted. A specially instrumented North American Rockwell OV-10 airplane was used to measure the wake and atmospheric conditions. An integrated database has been compiled for wake characterization and validation of wake vortex computational models. This paper describes the wake-measurement flight-data reduction process.

Introduction

Several of today's major airports are operating their capacity limit, leading to an increase in airport congestion and delays. As more and more airplanes are placed into the terminal area the probability of encountering wake turbulence is increased. A wake vortex upset is most hazardous for aircraft near the ground during landing and takeoff. The degree of upset mainly depends on the relative sizes of the vortex generating and vortex encountering airplanes, and the extent of wake decay. The rate of wake decay is highly dependent on the atmospheric state.

Numerous laboratory experiments and analytical models have been developed to study and simulate wake vortex flow physics. However, there is very little full-scale data available for comparison with and validation of the experimental and computational results. Many of the previous wake-measurement flight tests have omitted the atmospheric state data, which has a direct influence on wake flow physics. The National Aeronautics and Space Administration (NASA) conducted a series of flight tests to develop a wake-measurement data set with the accompanying atmospheric state information. This data set has been compiled into a database that can be used by wake vortex researchers to compare with experimental and computational results. Details of the database are provided in reference 1. This report describes the wake-measurement flight-data reduction process.

Symbols

| | |
|--|--|
| a | speed of sound, fps |
| b_{C130} | wing span of C-130, ft |
| b_{α} | angle of attack position error calibration bias, deg |
| b_{β} | sideslip position error calibration bias, deg |
| $b_{\Delta Pq}$ | position error pressure correction bias, psi |
| $b_{\Delta Pq\beta_n}$ | nose-boom position error pressure correction due to sideslip bias, psi |
| $b_{\Delta Pq\beta_1}, b_{\Delta Pq\beta_2}$ | wing-boom position error pressure correction due to sideslip bias terms, psi |
| b_{η} | flank angle position error calibration bias, deg |
| C_a | 5-hole probe angle of attack calibration curve coefficient |

| | |
|---------------|--|
| C_b | 5-hole probe sideslip calibration curve coefficient |
| Cor_E | east velocity integration correction factor |
| Cor_N | north velocity integration correction factor |
| Cor_Z | vertical velocity integration correction factor |
| C_q | dynamic pressure calibration coefficient |
| C_s | static pressure calibration coefficient |
| C_α | 5-hole probe angle of attack coefficient |
| C_β | 5-hole probe sideslip coefficient |
| d_E | distance east of wake origin, ft |
| $d_{E_{GPS}}$ | east distance computed from GPS, ft |
| $d_{E_{INS}}$ | east distance computed from integrated inertial velocity, ft |
| d_{E_o} | wake origin east offset distance, ft |
| d_N | distance north of wake origin, ft |
| $d_{N_{GPS}}$ | north distance computed from GPS, ft |
| $d_{N_{INS}}$ | north distance computed from integrated inertial velocity, ft |
| d_{N_o} | wake origin north offset distance, ft |
| d_{wk} | wake drift distance, ft |
| d_Z | vertical distance below wake origin, ft |
| $d_{Z_{GPS}}$ | vertical distance computed from GPS, ft |
| $d_{Z_{INS}}$ | vertical distance computed from integrated inertial velocity, ft |
| d_{Z_o} | wake origin vertical offset distance, ft |
| $drift_x$ | longitudinal wake drift distance in wake axis system, ft |
| $drift_y$ | lateral wake drift distance in wake axis system, ft |
| \dot{E} | airplane inertial velocity component east, fps |
| g | gravitational acceleration, 32.2 ft/s ² |

| | |
|--|--|
| h | altitude, ft |
| h_{grnd} | altitude at the ground, ft |
| h_{pass} | altitude of a pass, ft |
| HI | GPS geometric altitude, meters |
| i | array index variable |
| j | array index variable |
| k_{α} | linear slope of angle of attack position error calibration |
| k_{β} | linear slope of sideslip position error calibration |
| $k_{\Delta Pq}$ | linear slope of position error pressure correction |
| $k_{\Delta Pq\beta_n}$ | linear slope of nose-boom position error pressure correction due to sideslip |
| $k_{\Delta Pq\beta_1}, k_{\Delta Pq\beta_2}$ | linear slope of wing-boom position error pressure correction due to sideslip |
| k_{η} | linear slope of flank angle position error calibration |
| K | temperature recovery factor (0.995) |
| Lat | latitude, deg |
| Lat_a | latitude of point a , deg |
| Lat_b | latitude of point b , deg |
| $Lat_{C_{ref}}$ | latitude of C-130 at t_{ref} , deg |
| Lat_N | latitude north, deg |
| Lat_o | latitude of wake origin location, deg |
| $Lat_{OV_{ref}}$ | latitude of OV-10 at t_{ref} , deg |
| $Lat_{OV_{start}}$ | latitude of OV-10 at t_{start} , deg |
| $Lat_{OV_{stop}}$ | latitude of OV-10 at t_{stop} , deg |
| Lng | longitude, deg |
| Lng_a | longitude of point a , deg |
| Lng_b | longitude of point b , deg |

| | |
|--------------------|---|
| $Lng_{C_{ref}}$ | longitude of C-130 at t_{ref} , deg |
| Lng_o | longitude of wake origin location, deg |
| $Lng_{OV_{ref}}$ | longitude of OV-10 at t_{ref} , deg |
| $Lng_{OV_{start}}$ | longitude of OV-10 at t_{start} , deg |
| $Lng_{OV_{stop}}$ | longitude of OV-10 at t_{stop} , deg |
| Lng_W | longitude west, deg |
| M | Mach number |
| Mag_{var} | magnetic variation |
| \dot{N} | airplane inertial velocity component north, fps |
| $Outfile$ | Wake_Vel output file name |
| p_m | roll rate from mechanical gyro, deg/sec |
| $PDOP$ | dilution of precision parameter |
| P_o | standard sea-level static pressure, 2116.22 psf |
| P_{ref} | reference pressure, 1000 millibars |
| P_s | static pressure, psi |
| P_{s_c} | probe calibration corrected static pressure, psi |
| P_{s_o} | static pressure corrected for zero bias, psi |
| P_3 | 5-hole probe center port pressure, psi |
| $P_{\alpha 1}$ | 5-hole probe bottom port pressure, psi |
| $P_{\alpha 2}$ | 5-hole probe top port pressure, psi |
| $P_{\beta 1}$ | 5-hole probe right port pressure, psi |
| $P_{\beta 2}$ | 5-hole probe left port pressure, psi |
| q | dynamic pressure, psi |
| q_c | probe calibration corrected dynamic pressure, psi |
| q_m | pitch rate from mechanical gyro, deg/sec |

| | |
|-------------------|---|
| q_o | dynamic pressure corrected for zero bias, psi |
| r_m | yaw rate from mechanical gyro, deg/sec |
| R | gas constant, 1716.5 ft lb/(slug °R) |
| RMS | root mean squared position error, meters |
| Rng | range from one point to another, n. mi. |
| Rng_{err} | range error, n. mi. |
| Rng_{min} | minimum range error value, n. mi. |
| SV | number of navigation satellites received |
| t | time, sec |
| t_{GPS} | global positioning system time, sec |
| t_o | time when encountered wake was generated, sec |
| t_{pass} | time of pass, sec |
| t_{start} | event start time, sec |
| t_{stop} | event stop time, sec |
| t_{ref} | time of vortex encounter, sec |
| T_{abs} | absolute total air temperature, °R |
| \mathbf{T}_{be} | body axis to Earth axis transformation matrix |
| \mathbf{T}_{ew} | Earth axis to wake axis transformation matrix |
| T_m | total air temperature, °C |
| T_o | standard sea-level temperature, 518.67 °R |
| T_θ | potential temperature, °R |
| T_∞ | free-stream air temperature, °R |
| u_b | body-axis longitudinal airspeed component, fps |
| u_e | Earth-axis longitudinal airspeed component, fps |
| v_b | body-axis lateral airspeed component, fps |

| | |
|-----------------------------|--|
| v_e | Earth-axis lateral airspeed component, fps |
| V_{rtx} | vortex identifier (L for left, R for right) |
| V_t | true airspeed, fps |
| $V_{t_{loc}}$ | local true airspeed, fps |
| V_{wnd} | wind speed, knots |
| w_b | body-axis vertical airspeed component, fps |
| w_e | Earth-axis vertical airspeed component, fps |
| W_E | Earth-axis easterly wind component, fps |
| W_N | Earth-axis northerly wind component, fps |
| $W_{nd_{Dir}}$ | wind direction, degrees magnetic |
| W_{nd_E} | easterly wind component, fps |
| W_{nd_N} | northerly wind component, fps |
| $W_{nd_{Spd}}$ | wind speed, knots |
| W_{nd_x} | longitudinal wind component in the wake axis system, fps |
| W_{nd_y} | lateral wind component in the wake axis system, fps |
| W_Z | Earth-axis vertical wind component, fps |
| x, y, z | airplane axis coordinates, ft |
| x_b, y_b, z_b | airplane axis coordinates of the body-axis origin, ft |
| $x_{o_w}, y_{o_w}, z_{o_w}$ | wake axis coordinates of the body-axis origin, ft |
| Z | geometric altitude, ft |
| Z_o | geometric altitude of wake origin location, ft |
| $Z_{OV_{start}}$ | geometric altitude of OV-10 at t_{start} , ft |
| $Z_{OV_{stop}}$ | geometric altitude of OV-10 at t_{stop} , ft |
| \dot{Z} | airplane inertial velocity component up, fps |
| α | angle of attack, deg |

| | |
|------------------------|---|
| α_t | angle of attack corrected for airplane rotation rates, deg |
| α_{Vn} | wing tip alpha vane measurement, deg |
| β | sideslip angle, deg |
| β_t | sideslip angle corrected for airplane rotation rates, deg |
| β_{Vn} | wing tip beta vane measurement, deg |
| γ | specific heat ratio for air, 1.40 |
| η | flank angle, deg |
| ξ | dummy variable |
| ρ | air density, slug/ft ³ |
| ρ_{grnd} | air density at the ground, slug/ft ³ |
| ρ_{mid} | air density at middle altitude, slug/ft ³ |
| ρ_o | standard sea-level air density, 0.0023769 slug/ft ³ |
| θ | pitch angle, deg |
| ϕ | roll angle, deg |
| ψ | yaw angle, deg |
| Ψ | heading, deg |
| Ψ_w | heading of wake axis system, deg |
| Ψ_{wnd} | wind direction, deg |
| ΔP_q | position-error pressure correction, psi |
| $\Delta P_{q\beta}$ | position-error pressure correction due to sideslip, psi |
| $\Delta P_{\alpha 12}$ | pressure difference between 5-hole probe bottom and top ports, psi |
| $\Delta P_{\beta 12}$ | pressure difference between 5-hole probe right and left ports, psi |
| $\Delta P_{3\alpha 1}$ | pressure difference between 5-hole probe center and bottom ports, psi |
| $\Delta P_{3\beta 1}$ | pressure difference between 5-hole probe center and right ports, psi |
| Δt | wake age, sec |

Subscripts

| | |
|--------------|-------------------------------|
| <i>abs</i> | absolute value |
| <i>avg</i> | average value |
| Bias | zero bias correction |
| C130 | C-130 value |
| <i>e</i> | Earth axis system |
| <i>Fit</i> | from least-squares linear fit |
| <i>grnd</i> | value at the ground |
| <i>l</i> | left boom |
| <i>mag</i> | degrees magnetic |
| <i>n</i> | nose boom |
| <i>pass</i> | value during a pass |
| <i>probe</i> | probe measured value |
| <i>r</i> | right boom |
| <i>ref</i> | reference value |
| <i>tip</i> | C-130 wing tip value |
| <i>w</i> | wake axis system |
| <i>wk</i> | wake value |
| <i>wnd</i> | wind |
| 5 | 5-hole probe |
| 93 | Litton LN-93 INU value |

Superscripts

| | |
|---|------------------------------|
| ` | raw, uncorrected measurement |
|---|------------------------------|

Abbreviations

| | |
|-----|----------|
| a/c | aircraft |
|-----|----------|

| | |
|----------|---|
| CPT | control position transducer |
| DAS | experimental data acquisition system |
| INU | inertial navigation unit |
| GPS | global positioning system |
| LAFB | Langley Airforce Base |
| NACA | National Advisory Committee for Aeronautics |
| NASA | National Aeronautics and Space Administration |
| PCM | pulse code modulation |
| OVDRA | OV-10 data reduction and analysis program |
| SCADC | standard central air-data computer |
| UTC | Coordinated Universal Time |
| Wake_Vel | wake velocity program |

Flight Test Overview

The objective of the wake-measurement flight tests was to develop a full-scale data set with the accompanying atmospheric state information. The tests used two NASA airplanes as illustrated in figure 1.

The NASA Wallops Flight Facility's Lockheed C-130, shown in figure 2, was the wake generator. It was outfitted with wing tip smokers to mark the wake. It weighed between 105,000 and 95,000 pounds during the test and has a wingspan of 132 feet 7 inches. The tests were all flown with the C-130 in the clean (flaps up, gear up) configuration.

The NASA Langley's North American Rockwell OV-10A measured the wake and atmospheric conditions. The OV-10 was equipped with a three-boom, flow-sensor arrangement to measure the flow field characteristics of the wake. The booms were located on each wing tip and the right side of the nose as shown in figure 3. The OV-10 instrumentation is described in more detail in the next section. The OV-10 flew through the wake at various downstream distances measuring the wake velocities and position. A picture of a wake taken from the video camera mounted on the left tail is shown in figure 4. The smoke clearly denotes the two vortices.

The general flight test procedure was as follows. The OV-10 would fly to the flight test area and begin a series of "weather" runs. These would begin with one or two "turbulence" runs, which were 2-minute, level, constant heading flight segments 1000 feet below the test altitude. The test altitude was generally 4000 or 5000 feet. This was followed by a "weather profile" run, which was a constant speed, constant heading climb from 1000 feet below to 500 feet above the test altitude. Another series turbulence runs would then follow 500 feet above the test altitude. After completing the weather runs the

OV-10 would rendezvous with the C-130 and begin a series of “wake measurement” runs. The C-130 would fly a constant speed and heading at the test altitude. The OV-10 measured the wake by flying slower than the C-130 and making a series of wake penetrations at increasing ranges behind the C-130. At the conclusion of a series of wake measurement runs an additional series of weather runs were then conducted.

OV-10 Instrumentation

Significant modifications to the OV-10 were required to convert it from a stock aircraft into a research platform. An overview of the development of the research systems and measurement capabilities of the OV-10 is presented in reference 2. The following section provides a summary of the research instrumentation and experimental data system.

General System

A data acquisition system (DAS) was developed to collect and convert the analog signals from the experimental sensors and convert them into digital form for display, transmission, and recording. The system could record approximately two hours of data from 150 parameters at data rates up to 128 Hz. The major experimental instrumentation components are labeled in figure 3. The sensor outputs were signal conditioned, multiplexed and digitized by a commercial 12-bit pulse code modulation (PCM) subsystem that features functional flexibility, programmability, and the ability to multiplex analog and digital signals into a serial format. Major components of the sensor suite include:

- time-code generator to provide an accurate time base for all flight measurements,
- ring-laser-gyro inertial navigation unit (INU),
- global positioning system (GPS),
- standard central air-data computer (SCADC),
- fast-response rate and attitude gyros,
- two pitot-static and flow-angle-measurement systems,
- 5-hole airspeed and flow-angle probe,
- temperature probes,
- dew-point sensor,
- video/audio cameras/recorders,
- control position transducers (CPTs).

Except for sensors, displays, and control panels, most of the equipment for the DAS system is installed in the OV-10 cargo bay. A removable main instrumentation pallet, designed to fit in the aft portion of the cargo bay and roll out onto a cart for system maintenance, was fabricated and populated with equipment (Figures 5a and b). The forward part of the cargo bay housed the majority of the navigation, avionics and display equipment (Figure 6).

Navigation Systems

Three satellite based navigation systems have been added to the OV-10. The first is a multi-

component system that supports the research measurements and includes a Litton LN-93 ring-laser gyro INU integrated with a Honeywell 3A GPS receiver and a CPU-140/A SCADC. All the components communicate with the PCM system via a MIL-standard 1553 data bus through an 80486-processor/33-MHz personal-computer bus controller. The INU updates the GPS in the event of satellite signal loss, but the GPS does not update the INU position estimate. The INU also is capable of providing aircraft accelerations, velocities, and attitudes. Supplemental measurements of the linear accelerations and angular rates are provided by a separate package of fast-response rate gyros and accelerometers. The components of the research navigation system reside in the forward cargo bay on fixed plates and are not part of the removable instrument pallet. The second GPS system is an Ashtech Z12 system capable of storing 4 hours of position and velocity data at 1 Hz data rate. The third navigation system entails a Garmin GPS 100 mounted in the forward cockpit, and enables the pilot to precisely navigate and/or set up research maneuvers.

Air-Data Systems

There are two air-data systems on the OV-10. One system is the SCADC previously described, which is coupled to the INU/GPS system. The second system is the three-component pitot, static, and flow-direction measurement system described here.

Sensors mounted on the tips of graphite-epoxy research booms facilitate air data measurements at both wingtips and the nose. As is customary, the booms were designed to place sensors as far ahead of the predicted aircraft upwash influence as possible, yet have enough lightness and stiffness (high natural frequency) to prevent unwanted vibration influence on the sensor measurements. Thermally-controlled Setra pressure transducers, located approximately at the base of each respective research boom, provide for enhanced accuracy in pressure measurements. Accelerometers mounted near the tips of these booms provide information on boom vibration.

A standard National Advisory Committee for Aeronautics (NACA) pitot-static probe with balsa angle of attack and sideslip vanes, shown in figure 7, was mounted at the end of each wingtip boom approximately one chord length in front of the wing leading edge. The static and total pressure ports were connected to the pressure transducers by 13 feet of 1/4-inch inside-diameter flexible tubing. The balsa vanes, which have a high natural frequency of about 0.18 Hz per knot of indicated airspeed in incompressible flow (reference 3), have a natural frequency of approximately 22 Hz at the nominal OV-10 airspeed of 120 knots.

A Rosemount Model 858 AJ 5-hole probe, shown in figure 8, was mounted at the end of the nose boom. The Rosemount probe provides the required pressure ports for determining flow direction, airspeed, and altimetry measurements at the nose. The five pressure ports at the tip of the probe and the ring of static pressure ports about 3.5 inches aft are connected to a manifold such that the following pressure differences between the ports shown in figure 8 are measured.

$$\Delta P_{\alpha 12}' = P_{\alpha 1} - P_{\alpha 2} \quad (\text{psi}) \quad (1)$$

$$\Delta P_{\beta 12}' = P_{\beta 1} - P_{\beta 2} \quad (\text{psi}) \quad (2)$$

$$\Delta P_{3\alpha 1}' = P_3 - P_{\alpha 1} \quad (\text{psi}) \quad (3)$$

$$\Delta P_{3\beta 1}' = P_3 - P_{\beta 1} \quad (\text{psi}) \quad (4)$$

$$q_n' = P_3 - P_{s_n} \quad (\text{psi}) \quad (5)$$

The tip of the mounted probe is approximately 6 feet in front of the aircraft nose and approximately 2 feet to the right of the longitudinal centerline. The probe was connected to the pressure transducers by approximately 17 feet of 3/16-inch inside-diameter flexible tubing. A small 0.067-inch inside diameter restrictor was inserted in each 3/16 tubing near the 5-hole probe. The restrictor size was experimentally selected per reference 4 to provide maximum damping to the pressure oscillations measured by the transducers when a 20 Hz sinusoidal pressure was applied to the probe.

A pair of Rosemount Model 102 non-deiced total temperature probes (one for the SCADC and one for the research system) and a General Eastern 1011 Aircraft Dew-Point Sensor are also integrated into the air-data system. The temperature probes are located on the underside of the wing approximately midway between each engine and wingtip. The dew-point sensor is mounted on the left side of the forward fuselage.

Airborne Video/Audio Systems

The research instrumentation includes a video/audio system consisting of three miniature lipstick-size Elmo video cameras and three recorders. One camera is located at the tip of the left vertical tail, pointing in the general direction of flight, and includes the top of the wing and fuselage in its field of view, as shown in figure 4. This camera provides a good, qualitative means of reviewing the highlights of a flight in preparation for data reduction and analysis. The other two cameras are mounted near the tip of each wing and are pointed vertically downward. The wing tip cameras provide a stereo recording capability that is post-processed to compute the spacing between the vortex smoke trails and distance from the OV-10. Audio channels on the video/audio system enable the pilot and flight test engineer to record verbal data during maneuvers.

Flight Data Reduction Process

The basic data flow of the flight data reduction process is shown in figure 9. From each flight four data products are generated directly from the OV-10.

- Time-tagged, video recordings from the tail camera and both wing-tip cameras.
- Flight notes from the test pilot and flight engineers of event times and conditions
- Time-tagged data tape from the experimental data system
- Ashtech differential GPS data

The flight notes and video data are reviewed and used to establish a precise log of event times and test conditions called the “flight event” file. This information is then used to extract from the experimental data tape the pre and post-flight instrument calibration data and data from special calibration flight maneuvers. This calibration data is used to establish the instrumentation zero bias values, which are saved as a “flight constants” file for each flight. The event and constants files and the data from the DAS are input for the **OV-10 Data Reduction and Analysis Program (OVDRA)**. This program applies the instrument calibration and bias corrections to the DAS data and computes the inertial referenced wind components. Details of the OVDRA algorithms are presented in the *Calibration and Bias Corrections*

section of this report. The output of OVDRA is a calibrated data file for each run of the test flight. These run data files are used to characterize the atmosphere through wind and temperature profiles and turbulence calculations.

The wake velocity measurements are computed from the OVDRA output, the flight event file and the GPS position data from the OV-10 and the C-130. This information is input to the Wake Velocity Program (Wake_Vel) which computes the origin and age of the wake and translates the wind measurements to the wake axis system. Details of the Wake_Vel algorithms and the wake axis system are provided in the *Wake Velocity Calculation* section. The output of the Wake_Vel program is a data file for each wake measurement event of each run of each flight.

The pilot notes from the C-130 are used to estimate the initial circulation strength of the wake, which is required for subsequent wake decay analysis.

Calibration and Bias Corrections

The instrument calibrations and bias corrections are applied to the DAS data through the OVDRA program. All the recorded DAS data parameters are listed in table 1 along with their symbol and database name. All the data are interpolated to the highest sampling rate of 128 Hz. The sampling rates of all parameters are listed in the table. Those data parameters that do not have a symbol representation in table 1 are not used in the data reduction algorithms.

One of the primary functions of the OVDRA program is to translate the OV-10 atmospheric measurements from the airplane or body axis reference system, shown in figure 10 to an inertial reference system. This transformation is made through the yaw (ψ), pitch (θ), and roll (ϕ) Euler angles shown in figure 11.

The OVDRA program reads the DAS data at each time step and applies the following calculations.

Zero bias corrections

First the zero bias corrections are applied to the following parameters. The bias values were determined from pre-flight measurements with the airplane stationary in the hanger. These corrections compensate for shifts produced by the DAS signal conditioning circuitry.

- The static and dynamic pressure measurements from the left, nose and right booms, respectively.

$$P_{s_{oj}} = P_{s_j}' - P_{s_{j\text{Bias}}} \quad (\text{psi})$$

$$j = l, n, r$$
(6)

$$q_{oj} = q_j' - q_{j\text{Bias}} \quad (\text{psi})$$

$$j = l, n, r$$
(7)

- The pressure difference measurements across the nose boom 5-hole probe.

$$\Delta P_{\alpha 12} = \Delta P_{\alpha 12}' - \Delta P_{\alpha 12\text{Bias}} \quad (\text{psi})$$
(8)

$$\Delta P_{\beta 12} = \Delta P_{\beta 12}' - \Delta P_{\beta 12 \text{Bias}} \quad (\text{psi}) \quad (9)$$

$$\Delta P_{3\alpha 1} = \Delta P_{3\alpha 1}' - \Delta P_{3\alpha 1 \text{Bias}} \quad (\text{psi}) \quad (10)$$

$$\Delta P_{3\beta 1} = \Delta P_{3\beta 1}' - \Delta P_{3\beta 1 \text{Bias}} \quad (\text{psi}) \quad (11)$$

- The mechanical gyro measurements of roll, pitch and yaw rates, respectively.

$$p_m = p_m' - p_{m \text{Bias}} \quad (\text{deg/sec}) \quad (12)$$

$$q_m = q_m' - q_{m \text{Bias}} \quad (\text{deg/sec}) \quad (13)$$

$$r_m = r_m' - r_{m \text{Bias}} \quad (\text{deg/sec}) \quad (14)$$

- The total temperature measurement.

$$T_m = T_m' - T_{m \text{Bias}} \quad (^\circ \text{C}) \quad (15)$$

Rosemont 5-Hole Probe Calibration Correction

The first step in the 5-hole probe calibration correction is to compute the angle-of-attack and sideslip coefficients

$$C_\alpha = \frac{\Delta P_{\alpha 12}}{\frac{1}{2}(\Delta P_{3\beta 1} + \Delta P_{3\alpha 1}) + \frac{1}{4}(\Delta P_{\beta 12} + \Delta P_{\alpha 12})} \quad (16)$$

$$C_\beta = \frac{\Delta P_{\beta 12}}{\frac{1}{2}(\Delta P_{3\beta 1} + \Delta P_{3\alpha 1}) + \frac{1}{4}(\Delta P_{\beta 12} + \Delta P_{\alpha 12})} \quad (17)$$

A fifth-order two-dimensional polynomial calibration curve that is a function of C_α and C_β is then used to compute the local angle of attack and sideslip.

$$\alpha_5 = \sum_{i=0}^4 \sum_{j=0}^4 C_\alpha^j \cdot C_\beta^i \cdot C_{a_{5i+j+1}} \quad (\text{deg}) \quad (18)$$

$$\beta_5 = \sum_{i=0}^4 \sum_{j=0}^4 C_\alpha^j \cdot C_\beta^i \cdot C_{b_{5i+j+1}} \quad (\text{deg}) \quad (19)$$

The local dynamic and static pressure are computed in a similar manner.

$$q_5 = \frac{q_{o_n}}{1 - \sum_{i=0}^4 \sum_{j=0}^4 C_{\alpha}^j \cdot C_{\beta}^i \cdot C_{q_{5i+j+1}}} \quad (\text{psi}) \quad (20)$$

$$Ps_5 = Ps_{o_n} + q_5 \sum_{i=0}^4 \sum_{j=0}^4 C_{\alpha}^j \cdot C_{\beta}^i \cdot C_{s_{5i+j+1}} \quad (\text{psi}) \quad (21)$$

The values for the polynomial coefficients C_a , C_b , C_q and C_s were derived from proprietary manufacturer's data and independent wind tunnel tests.

Position Error Corrections to Local Flow Angle Measurements

The position error correction terms were derived from the airspeed calibration tests that are discussed in appendix A. The corrections to the local angle of attack measurements are:

$$\alpha_r = k_{\alpha_r} \cdot \alpha_{Vn_r} + b_{\alpha_r} \quad (\text{deg}) \quad (22)$$

$$\alpha_l = k_{\alpha_l} \cdot \alpha_{Vn_l} + b_{\alpha_l} \quad (\text{deg}) \quad (23)$$

$$\alpha_n = k_{\alpha_n} \cdot \alpha_5 + b_{\alpha_n} \quad (\text{deg}) \quad (24)$$

The vertical balsa vanes on the wing tip booms that are referred to as the sideslip or β vanes actually measure the flank angle rather than the true sideslip. The position corrections to the flank angle measurements are:

$$\eta_r = k_{\eta_r} \cdot \beta_{Vn_r} + b_{\eta_r} \quad (\text{deg}) \quad (25)$$

$$\eta_l = k_{\eta_l} \cdot \beta_{Vn_l} + b_{\eta_l} \quad (\text{deg}) \quad (26)$$

The sideslip angles are computed from the flank angle measurements through the trigonometric relationship.

$$\beta_j = \tan^{-1}(\tan \eta_j \cos \alpha_j) \quad (\text{deg}) \quad (27)$$

$j = r, l$

The position correction for the nose boom sideslip measurement is:

$$\beta_n = k_{\beta_n} \cdot \beta_5 + b_{\beta_n} \quad (\text{deg}) \quad (28)$$

The baseline values for the position error correction terms (i.e. the k and b terms) are provided in table 2, which lists all the calibration constants. The b terms are modified for each flight based on data from pre and post-flight calibrations and in-flight calibration maneuvers.

NACA Pitot Probe Calibration Corrections

The NACA pitot probe measurements from each wing tip boom are corrected for local flow angle effects based on wind tunnel calibration data. The static and dynamic pressure correction coefficients, C_s and C_q respectively, are obtained from a 2-D table lookup as a function of the local angle of attack and sideslip. Tables 3 and 4 list the C_s and C_q coefficient values, respectively, as a function of the local angle of attack and sideslip. The dynamic and static pressure corrections are:

$$q_{c j} = \frac{q_{o j}}{1 - C_{q j}} \quad (29)$$

$$j = r, l$$

$$P_{s c j} = P_{s o j} + C_{s j} \cdot q_{c j} \quad (30)$$

$$j = r, l$$

Position Error Corrections to Static and Dynamic Pressure Measurements

The position-error pressure correction terms were determined from the airspeed calibration tests and are developed in Appendix A. The correction terms were found to be a function of the local dynamic pressure and sideslip. The pressure correction terms are computed as:

$$\Delta P_{q j} = k_{\Delta P_{q j}} \cdot q_{c j} + b_{\Delta P_{q j}} + \Delta P_{q \beta j} \quad (\text{psi}) \quad (31)$$

$$j = r, l$$

$$\Delta P_{q_n} = k_{\Delta P_{q_n}} \cdot q_5 + b_{\Delta P_{q_n}} + \Delta P_{q \beta_n} \quad (\text{psi}) \quad (32)$$

where the sideslip correction is:

$$\Delta P_{q \beta_n} = \text{Min} \left(0, k_{\Delta P_{q \beta_n}} \cdot |\beta_n| + b_{\Delta P_{q \beta_n}} \right) \quad (\text{psi}) \quad (33)$$

$$\Delta P_{q \beta_r} = \begin{cases} k_{\Delta P_{q \beta_1}} \cdot \beta_r + b_{\Delta P_{q \beta_1}} & , \beta_r < 0 \\ k_{\Delta P_{q \beta_2}} \cdot \beta_r + b_{\Delta P_{q \beta_2}} & , \beta_r \geq 0 \end{cases} \quad (\text{psi}) \quad (34)$$

$$\Delta P_{q \beta_l} = \begin{cases} -k_{\Delta P_{q \beta_2}} \cdot \beta_l + b_{\Delta P_{q \beta_2}} & , \beta_l < 0 \\ -k_{\Delta P_{q \beta_1}} \cdot \beta_l + b_{\Delta P_{q \beta_1}} & , \beta_l \geq 0 \end{cases} \quad (\text{psi}) \quad (35)$$

The position error pressure correction is applied to the static and dynamic pressure through:

$$P_{s j} = P_{s c j} - \Delta P_{q j} \quad (\text{psi}) \quad (36)$$

$$j = r, l$$

$$P_{s_n} = P_{s_5} - \Delta P_{q_n} \quad (\text{psi}) \quad (37)$$

$$q_j = q_{cj} + \Delta P q_j \quad (\text{psi})$$

$$j = r, l$$
(38)

$$q_n = q_5 + \Delta P q_n \quad (\text{psi})$$
(39)

Local Mach Number Calculation

After all the corrections are applied to the static and dynamic pressure measurements the local Mach number at each boom is computed from:

$$M_j = \sqrt{\left(\frac{2}{\gamma - 1} \right) \left[\left(\frac{q_j}{P_{sj}} + 1 \right)^{\frac{\gamma - 1}{\gamma}} - 1 \right]}$$

$$j = n, r, l$$
(40)

where the ratio of specific heats (γ) for air is 1.40. The average local Mach number is then computed as:

$$M_{avg} = \frac{1}{3} (M_n + M_r + M_l)$$
(41)

Free-Air Temperature and Speed of Sound Calculation

The measured temperature is converted from degrees Celsius to absolute temperature in degrees Rankine.

$$T_{abs} = \frac{9}{5} \cdot T_m + 32 + 459.67 \quad (^\circ \text{R})$$
(42)

The free-stream air temperature is then computed from the local absolute temperature as:

$$T_\infty = \frac{T_{abs}}{1 + \left[\left(\frac{\gamma - 1}{2} \right) \cdot K \cdot M_{avg}^2 \right]} \quad (^\circ \text{R})$$
(43)

where the temperature recovery factor (K) is 0.995. The potential temperature is computed as:

$$T_\theta = T_\infty \left(\frac{P_{ref}}{P_{sn} \cdot 68.9475} \right)^{\frac{2}{\gamma}} \quad (^\circ \text{R})$$
(44)

where the reference pressure (P_{ref}) is 1000 millibars.

The free-stream speed of sound is computed from:

$$a = \sqrt{\gamma \frac{P_o}{\rho_o} \frac{T_\infty}{T_o}} \quad (\text{fps})$$
(45)

where:

$$\begin{aligned} P_o &= 2116.22 \quad (\text{lb/ft}^2) \\ \rho_o &= 0.0023769 \quad (\text{slug/ft}^3) \\ T_o &= 518.67 \quad (^\circ \text{R}) \end{aligned}$$

The local true airspeed is computed from the local Mach number and the free-stream speed of sound.

$$\begin{aligned} V_{tloc_j} &= M_j \cdot a \quad (\text{fps}) \\ j &= n, r, l \end{aligned} \quad (46)$$

Airplane Angular Motion Correction to Body Axis Airspeed Components

The body-axis airspeed components are computed and corrected for the airplane angular motions as:

$$\begin{aligned} u_{b_j} &= V_{tloc_j} \cos \alpha_j \cos \beta_j + \frac{\pi}{180} [r_m(y_j - y_b) - q_m(z_j - z_b)] \quad (\text{fps}) \\ j &= n, r, l \end{aligned} \quad (47)$$

$$\begin{aligned} v_{b_j} &= V_{tloc_j} \sin \beta_j + \frac{\pi}{180} [p_m(z_j - z_b) - r_m(x_j - x_b)] \quad (\text{fps}) \\ j &= n, r, l \end{aligned} \quad (48)$$

$$\begin{aligned} w_{b_j} &= V_{tloc_j} \sin \alpha_j \cos \beta_j + \frac{\pi}{180} [q_m(x_j - x_b) - p_m(y_j - y_b)] \quad (\text{fps}) \\ j &= n, r, l \end{aligned} \quad (49)$$

The airplane axis x, y and z coordinates of the boom probes and body axis origin (x_b, y_b, z_b) are listed in Table 5. The angular rates (p_m, q_m, r_m) are from the mechanical gyros and are sampled at 32 times per second while the velocity parameters are sampled at 128 times per second. The angular rates are interpolated in the missing time slots (3 points between each sample). The angular rates from the mechanical gyros were selected over the LN-93 INU rates due to a dithering of the INU rate signals.

True Airspeed, Angle Of Attack and Sideslip Calculation

The true airspeed at each boom is computed as:

$$\begin{aligned} V_{t_j} &= \sqrt{u_{b_j}^2 + v_{b_j}^2 + w_{b_j}^2} \quad (\text{fps}) \\ j &= n, r, l \end{aligned} \quad (50)$$

The angle of attack at each boom is computed as:

$$\begin{aligned} \alpha_{t_j} &= \frac{180}{\pi} \tan^{-1} \left(\frac{w_{b_j}}{u_{b_j}} \right) \quad (\text{deg}) \\ j &= n, r, l \end{aligned} \quad (51)$$

The sideslip angle at each boom is computed as:

$$\beta_{t_j} = \frac{180}{\pi} \sin^{-1} \left(\frac{v_{b_j}}{V_{t_j}} \right) \quad (\text{deg})$$

$$j = n, r, l \quad (52)$$

The average airspeed components and flow angles are then computed.

$$V_{t_{avg}} = \frac{1}{3} (V_{t_n} + V_{t_r} + V_{t_l}) \quad (\text{fps}) \quad (53)$$

$$u_{b_{avg}} = \frac{1}{3} (u_{b_n} + u_{b_r} + u_{b_l}) \quad (\text{fps}) \quad (54)$$

$$v_{b_{avg}} = \frac{1}{3} (v_{b_n} + v_{b_r} + v_{b_l}) \quad (\text{fps}) \quad (55)$$

$$w_{b_{avg}} = \frac{1}{3} (w_{b_n} + w_{b_r} + w_{b_l}) \quad (\text{fps}) \quad (56)$$

$$\alpha_{avg} = \frac{1}{3} (\alpha_{t_n} + \alpha_{t_r} + \alpha_{t_l}) \quad (\text{deg}) \quad (57)$$

$$\beta_{avg} = \frac{1}{3} (\beta_{t_n} + \beta_{t_r} + \beta_{t_l}) \quad (\text{deg}) \quad (58)$$

Calculation of Wind Components in Earth Axis System

The airspeed components are transformed from the body axis system to the Earth axis system through transformation equation:

$$\begin{pmatrix} u_{e_j} \\ v_{e_j} \\ w_{e_j} \end{pmatrix} = \mathbf{T}_{be} \begin{pmatrix} u_{b_j} \\ v_{b_j} \\ w_{b_j} \end{pmatrix} \quad (\text{fps})$$

$$j = n, r, l, avg \quad (59)$$

where the transformation matrix (\mathbf{T}_{be}) is defined as:

$$\mathbf{T}_{be} = \begin{pmatrix} \cos \psi_{93} \cos \theta_{93} & \cos \psi_{93} \sin \theta_{93} \sin \phi_{93} & \cos \psi_{93} \sin \theta_{93} \cos \phi_{93} \\ \sin \psi_{93} \cos \theta_{93} & \sin \psi_{93} \sin \theta_{93} \sin \phi_{93} & \sin \psi_{93} \sin \theta_{93} \cos \phi_{93} \\ -\sin \theta_{93} & \cos \theta_{93} \sin \phi_{93} & \cos \theta_{93} \cos \phi_{93} \end{pmatrix} \quad (60)$$

The inertial wind components are computed as the difference between the airplane inertial velocity

and the measured airspeed components.

$$W_{N_j} = \dot{N} - u_{e_j} \quad (\text{fps})$$

$$j = n, r, l, \text{avg} \quad (61)$$

$$W_{E_j} = \dot{E} - v_{e_j} \quad (\text{fps})$$

$$j = n, r, l, \text{avg} \quad (62)$$

$$W_{Z_j} = -\dot{Z} - w_{e_j} \quad (\text{fps})$$

$$j = n, r, l, \text{avg} \quad (63)$$

Average Wind Speed and Direction Calculation

The average horizontal wind components are computed as:

$$W_{N_{avg}} = \frac{1}{3} (W_{N_l} + W_{N_n} + W_{N_r}) \quad (\text{fps}) \quad (64)$$

$$W_{E_{avg}} = \frac{1}{3} (W_{E_l} + W_{E_n} + W_{E_r}) \quad (\text{fps}) \quad (65)$$

The wind speed and direction are then computed from:

$$W_{nd_{Spd}} = 0.5925 \sqrt{W_{N_{avg}}^2 + W_{E_{avg}}^2} \quad (\text{knots}) \quad (66)$$

$$W_{nd_{Dir}} = 180 + \tan^{-1} \left(\frac{W_{E_{avg}}}{W_{N_{avg}}} \right) \quad (\text{deg true}) \quad (67)$$

At the conclusion of the above calculations the DAS input data and selected computed parameters are recorded. Table 6 lists the recorded parameters and cross-references the equation where they are computed. The data for the next time step is read and the calculation process begins again at equation 6. This process loop is repeated until the end of the DAS file is reached.

Wake Velocity Calculation

The following process was used to derive the wake velocity measurements from the OVDRA output, the flight event information, and the GPS position data from the OV-10 and the C-130. The objective of the wake measurement flight tests was to obtain a “real world” data set for use in wake modeling analysis. The ideal data set for such analysis would be a series of instantaneous, 3-dimensional wake measurements within a fixed airmass, from initial wake rollup until final decay. However, currently there is no way to make such measurements. The OV-10 could only measure the wake velocity at 3-points in space at any instant in time. A wake measurement pass consists of 3 streams of wake velocity data collected at 128 Hz, over a 5 to 10 second period. Successive wake measurements were made in different airmass regions rather than an ideal fixed airmass. The OV-10 and C-130 inertial positions are known from differential GPS measurements collected at 1 Hz. The following process was used to translate the measured wake velocity data to an inertial-referenced frozen axis system.

Wake Coordinate System

The wake vortex axis system (X_w, Y_w), shown in figure 12, is aligned with the bearing between the OV-10 and C-130 at the time of the wake vortex encounter (t_{ref}). The origin of the coordinate system is the C-130 position when it generated the wake being measured (C-130 position at t_o).

Wake Velocity Algorithm

The wake velocity algorithm Wake_Vel must translate the OVDRA wind measurements to the wake coordinate system. Each wake measurement event has its own wake coordinate system. As noted in the previous section, the origin of the coordinate system is the C-130 position (latitude, longitude, and altitude) when it generated the measured wake event. Since the wake translates with the airmass this origin location must be iteratively determined based on the known C-130 track and OV-10 measurement location, and the average wind component determined from measurements outside the wake. The wake origin location also determines the wake age.

Filtering GPS position data. The wake velocity algorithm begins by reading and filtering the OV-10 and C-130 Ashtech differential GPS data files for a given flight. The read and filter operations are the same for both the OV-10 and C-130 data. The following data parameters are read at each time step:

| | |
|-----------|--|
| t_{GPS} | GPS time, seconds |
| SV | Number of satellites received |
| $PDOP$ | Dilution of Precision Parameter |
| Lat_N | Latitude north, degrees |
| Lng_W | Longitude west, degrees |
| HI | Geometric altitude, meters |
| RMS | Root mean squared position error, meters |

The following criteria are used to filter poor position data from the GPS files. The data that do not meet the criteria are omitted.

$$\begin{aligned} RMS &\leq 1.0 \\ PDOP &\leq 4.0 \\ SV &\geq 4 \end{aligned} \tag{68}$$

For the remaining data, the GPS time is converted to Coordinated Universal Time (UTC) through:

$$t = \begin{cases} t_{GPS} - 10.0 & \text{for 1995 flights} \\ t_{GPS} - 11.0 & \text{for 1996 flights} \\ t_{GPS} - 12.0 & \text{for 1997 flights} \\ t_{GPS} - 26.7 & \text{for flight 705 (DAS time not reset)} \end{cases} \tag{69}$$

The longitude west is converted to longitude east, and the geometric altitude is converted to feet through:

$$Z = -3.281 * HI \quad (\text{ft}) \tag{70}$$

Begin wake velocity computation loop. The wake velocity computation loop begins with reading the

event data. The loop is repeated until the end of the event data is reached. The event information consists of:

| | |
|--------------|--|
| t_{start} | Event start time, UTC seconds |
| t_{stop} | Event stop time, UTC seconds |
| t_{ref} | Time of vortex encounter, UTC seconds |
| V_{rtx} | Vortex identifier (L for left, R for Right) corresponding to t_{ref} |
| V_{wnd} | Wind speed, knots |
| Ψ_{wnd} | Wind direction, degrees true |
| $Outfile$ | Wake_Vel output file name |

Find OV-10 locations corresponding to event start, stop and reference times. The first step in the computation loop is to interpolate the 1 Hz OV-10 GPS data to find the location corresponding to t_{start} , t_{stop} , and t_{ref} . The algorithm will not interpolate between points with data dropouts. If the time interval between a pair of GPS data points is greater than 1.2 seconds, then the data between those points did not meet the dropout check criteria. An error message stating that the GPS data is invalid over the interpolation region is written and the event output file is closed. The algorithm returns to the beginning of the loop to read the next event data.

Determine when C-130 generated the wake encountered. This is the beginning of a search-loop to determine when the C-130 generated the wake encountered. The search begins at the C-130 location corresponding to t_{ref} and searches backward to find the time (t_o) when the wake encounter position (corrected for the wind drift) is closest to the C-130 track. A flowchart of the search algorithm is shown in figure 13.

$$t_o = f\left(t_{ref}, Lat_{OV_{ref}}, Lng_{OV_{ref}}, V_{rtx}, \Psi_{wnd}, V_{wnd}, C-130 \text{ GPS data}\right) \quad (71)$$

The algorithm, as depicted, finds the nearest C-130 data point corresponding to the wake generation point. The algorithm has a second iteration loop (not depicted for clarity) which interpolates between GPS data points to find the wake origin time to the nearest tenth of a second and corresponding location (Lat_o, Lng_o, Z_o). The search algorithm also uses several functions relating range and bearing between two latitude and longitude points which are not explicitly expressed in figure 13. These functions are given below.

The range from (Lat_a, Lng_a) to (Lat_b, Lng_b) is computed as:

$$Rng = 60 \frac{180}{\pi} \left[\frac{\pi}{2} + \tan^{-1} \left(\frac{-\xi}{\sqrt{1-\xi^2}} \right) \right] \quad (\text{n.mi.}) \quad (72)$$

where $\xi = \sin Lat_a \sin Lat_b + \cos Lat_a \cos Lat_b \cos(Lng_b - Lng_a)$

The bearing from (Lat_a, Lng_a) to (Lat_b, Lng_b) is computed as:

$$\Psi = \frac{180}{\pi} \left[\frac{\pi}{2} + \tan^{-1} \left(\frac{-\xi}{\sqrt{1-\xi^2}} \right) \right] \quad (\text{deg})$$

$$\text{where } \xi = \frac{\sin Lat_b - \sin Lat_a \cos \frac{Rng}{60}}{\cos Lat_a \sin \frac{Rng}{60}}$$
(73)

The latitude and longitude of a point at a given range (Rng in nautical miles) and bearing (Ψ) from an initial location (Lat_a, Lng_a) are computed from:

$$Lat = Lat_a + \frac{Rng}{60} \cos \Psi \quad (\text{deg})$$
(74)

$$Lng = Lng_a + \frac{Rng \sin \Psi}{60 \cos \left(\frac{Lat + Lat_a}{2 - 2 \cdot 10^{-6} Rng} \right)} \quad (\text{deg})$$
(75)

Compute wake age. At the conclusion of the search for t_o the wake age is computed from:

$$\Delta t = t_{ref} - t_o$$
(76)

Find C-130 location corresponding to event start and stop times. The C-130 GPS data is interpolated to find its location at $t_{start} - \Delta t$ and $t_{stop} - \Delta t$. As with the OV-10 GPS interpolation, the interpolation interval is checked for validity. If the time interval between interpolation data points is greater than 1.2 seconds, then the GPS data did not meet the dropout filter criteria over that region. An error message stating that the GPS data is invalid is written and the event output file is closed. The algorithm returns to the beginning of the loop to read the next event data.

Find C-130 location at the reference time. A linear extrapolation of the C-130 ground track from $t_{start} - \Delta t$ to $t_{stop} - \Delta t$ is used to compute its location at t_{ref} . The linear projection approach is used rather than interpolating the GPS data because at the end of the runs the C-130 often turns or enters a circular pattern until the OV-10 completes its wake measurements. Interpolating the GPS data for the C-130 position in such a situation will result in the wake axis system being misaligned.

Least squares linear fits of the C-130 GPS latitude and longitude as functions of time are computed from $t_{start} - \Delta t$ to $t_{stop} - \Delta t$. The projected latitude ($Lat_{C_{ref}}$) and longitude ($Lng_{C_{ref}}$) corresponding to t_{ref} are then computed from the linear fit.

Compute vortex initial location at the reference time. The vortex initial location at t_{ref} is assumed to be the left or right wing tip location of the C-130. The wing tip location at t_{ref} is computed as:

$$Lat_{tip}, Lng_{tip} = f \left(Lat_{C_{ref}}, Lng_{C_{ref}}, \Psi_{tip}, \frac{1}{2} b_{C130} \right)$$
(77)

using equations 74 and 75, respectively; where

$$\Psi_{tip} = \begin{cases} \Psi_{C130} + 90 & , Vrtx = R \text{ (right vortex)} \\ \Psi_{C130} - 90 & , Vrtx = L \text{ (left vortex)} \end{cases} \quad (78)$$

and

$$\Psi_{C130} = f[Lat_{C130}(t_{start} - \Delta t), Lng_{C130}(t_{start} - \Delta t), Lat_{C130}(t_{stop} - \Delta t), Lng_{C130}(t_{stop} - \Delta t)] \quad (79)$$

from equation 73.

Compute heading of wake axis system. The bearing from the OV-10 location at t_{ref} and the C-130 tip location at t_{ref} is the heading of the wake axis system. The wake axis heading is obtained as:

$$\Psi_w = f(Lat_{tip}, Lng_{tip}, Lat_{OV_{ref}}, Lng_{OV_{ref}}) \quad (80)$$

from equation 73.

Compute Earth to Wake axis transformation matrix. The Earth to wake axis system transformation matrix elements are computed as:

$$\mathbf{T}_{ew} = \begin{pmatrix} \cos \Psi_w & \sin \Psi_w & 0 \\ -\sin \Psi_w & \cos \Psi_w & 0 \\ 0 & 0 & 1 \end{pmatrix} \quad (81)$$

Compute OV-10 INS velocity integration correction factor. The OV-10 position at each 128 Hz data record is determined by integrating the LN-93 INS velocity components over the duration of the event. An integration correction factor is then calculated that forces the position calculations to match the 1 Hz Ashtech GPS position data.

The north, east and vertical distance traveled during the event are first computed by integrating the LN-93 velocities from t_{start} to t_{stop} .

$$d_{N_{INS}} = \sum_{t_{start}}^{t_{stop}} \frac{1}{2}(t_i - t_{i-1})(\dot{N}_i - \dot{N}_{i-1}) \quad (\text{ft}) \quad (82)$$

$$d_{E_{INS}} = \sum_{t_{start}}^{t_{stop}} \frac{1}{2}(t_i - t_{i-1})(\dot{E}_i - \dot{E}_{i-1}) \quad (\text{ft}) \quad (83)$$

$$d_{Z_{INS}} = \sum_{t_{start}}^{t_{stop}} -\frac{1}{2}(t_i - t_{i-1})(\dot{Z}_i - \dot{Z}_{i-1}) \quad (\text{ft}) \quad (84)$$

The range and bearing from the event starting location to the stop location are then computed from equations 72 and 73, respectively.

$$Rng, \Psi = f(Lat_{OV_{start}}, Lng_{OV_{start}}, Lat_{OV_{stop}}, Lat_{OV_{stop}}) \quad (85)$$

The north, east and vertical distances based on the OV-10 Ashtech GPS data are computed as:

$$d_{N_{GPS}} = 6076.1 \cdot Rng \cdot \cos \Psi \quad (\text{ft}) \quad (86)$$

$$d_{E_{GPS}} = 6076.1 \cdot Rng \cdot \sin \Psi \quad (\text{ft}) \quad (87)$$

$$d_{Z_{GPS}} = Z_{OV_{start}} - Z_{OV_{stop}} \quad (\text{ft}) \quad (88)$$

The north, east and vertical integration correction factors are then computed.

$$Cor_j = \frac{d_{j_{GPS}} - d_{j_{INS}}}{t_{stop} - t_{start}} \quad (89)$$

$j = N, E, Z$

Compute the event origin offset distances. The origin of the wake axis system is the location of the C-130 at t_0 (equation 71). The range and bearing from the event starting location to the C-130 initial location are computed from equations 72 and 73, respectively.

$$Rng, \Psi = f(Lat_{OV_{start}}, Lng_{OV_{start}}, Lat_o, Lng_o) \quad (90)$$

The origin-offset distances are then computed as:

$$d_{N_o} = 6076.1 \cdot Rng \cdot \cos \Psi \quad (\text{ft}) \quad (91)$$

$$d_{E_o} = 6076.1 \cdot Rng \cdot \sin \Psi \quad (\text{ft}) \quad (92)$$

$$d_{Z_o} = Z_{OV_{start}} - Z_o \quad (\text{ft}) \quad (93)$$

Compute OV-10 position and wind velocities in the wake axis system. The OV-10 position in the wake axis system is computed at each data record by integrating the INS velocities with the integration correction factors and origin offset. The measured wind velocities are also transformed to the wake axis system.

The INS velocity components are integrated with the correction factors and origin offsets for $t_{start} \leq t_i \leq t_{stop}$:

$$d_{N_i} = d_{N_o} + Cor_N(t_i - t_{start}) + \sum_{j=i_{start}}^i \frac{1}{2}(t_j - t_{j-1})(\dot{N}_j - \dot{N}_{j-1}) \quad (\text{ft}) \quad (94)$$

$$d_{E_i} = d_{E_o} + Cor_E(t_i - t_{start}) + \sum_{j=i_{start}}^i \frac{1}{2}(t_j - t_{j-1})(\dot{E}_j - \dot{E}_{j-1}) \quad (\text{ft}) \quad (95)$$

$$d_{Z_i} = d_{Z_o} + Cor_Z(t_i - t_{start}) + \sum_{j=i_{start}}^i -\frac{1}{2}(t_j - t_{j-1})(\dot{Z}_j - \dot{Z}_{j-1}) \quad (\text{ft}) \quad (96)$$

where i and i_{start} are the data array indices corresponding to t_i and t_{start} , respectively.

The distance components are then transformed to the wake axis system yielding the coordinates of the OV-10 body axis origin in the wake axis system.

$$\begin{pmatrix} x_{o_w} \\ y_{o_w} \\ z_{o_w} \end{pmatrix}_i = \mathbf{T}_{ew} \begin{pmatrix} d_N \\ d_E \\ d_Z \end{pmatrix}_i \quad (\text{ft}) \quad (97)$$

The boom coordinates in the Earth axis system are computed.

$$\begin{pmatrix} x_{j_e} \\ y_{j_e} \\ z_{j_e} \end{pmatrix}_i = \mathbf{T}_{be_i} \begin{pmatrix} x_j - x_b \\ y_j - y_b \\ z_j - z_b \end{pmatrix} \quad (\text{ft}) \quad (98)$$

$j = r, l, n$

where the components of the \mathbf{T}_{be} matrix are obtained from the OVDRA file at each time step.

The boom coordinates and wind measurements are then transformed to the wake axis system.

$$\begin{pmatrix} x_{j_w} \\ y_{j_w} \\ z_{j_w} \end{pmatrix}_i = \begin{pmatrix} x_{o_w} \\ y_{o_w} \\ z_{o_w} \end{pmatrix}_i + \mathbf{T}_{ew} \begin{pmatrix} x_{j_e} \\ y_{j_e} \\ z_{j_e} \end{pmatrix}_i \quad (\text{ft}) \quad (99)$$

$j = r, l, n$

$$\begin{pmatrix} u_{j_w} \\ v_{j_w} \\ w_{j_w} \end{pmatrix}_i = \mathbf{T}_{ew} \begin{pmatrix} W_{N_j} \\ W_{E_j} \\ W_{Z_j} \end{pmatrix}_i \quad (\text{fps}) \quad (100)$$

$j = r, l, n$

Wake position correction for wind drift. This correction is made in an effort to obtain an instantaneous sample of the wake velocity flow-field. Since a wake measurement pass requires a number of seconds to complete, the measurement positions must be corrected to account for the drift of the wake over the measurement period.

First, the average wind, which is one of the inputs to the Wake_Vel algorithm, is translated to the wake axis system.

$$\begin{pmatrix} Wnd_x \\ Wnd_y \\ 0 \end{pmatrix} = \mathbf{T}_{ew} \begin{pmatrix} Wnd_N \\ Wnd_E \\ 0 \end{pmatrix} \quad (\text{fps}) \quad (101)$$

where

$$\begin{pmatrix} Wnd_N \\ Wnd_E \end{pmatrix} = 1.688 \cdot V_{wnd} \cdot \begin{pmatrix} \cos(\Psi_{wnd} - 180) \\ \sin(\Psi_{wnd} - 180) \end{pmatrix} \quad (\text{fps}) \quad (102)$$

Each point in the measurement pass is then corrected for wind drift relative to the position at t_{ref} .

$$\begin{pmatrix} x_{j_w} \\ y_{j_w} \end{pmatrix}_i = \begin{pmatrix} x_{j_w} \\ y_{j_w} \end{pmatrix}_i - \begin{pmatrix} drift_x \\ drift_y \end{pmatrix} \quad (\text{ft}) \quad (103)$$

$j = r, l, n$

where

$$\begin{pmatrix} drift_x \\ drift_y \end{pmatrix} = (t_i - t_{ref}) \begin{pmatrix} Wnd_x \\ Wnd_y \end{pmatrix} \quad (\text{ft}) \quad (104)$$

Write wake velocities and positions to output file. The wake velocities and positions at each boom are written to the output file *Outfile*.

Closing Remarks

This paper has described and documented the flight-data reduction process for a series of flight tests that were conducted to measure airplane wake and atmospheric state information. A specially instrumented North American Rockwell OV-10 airplane was used to measure the wake and atmospheric conditions. A Lockheed C-130 airplane was used to generate the wake. An integrated database has been compiled for wake characterization and validation of wake vortex computational models.

References

1. Vicroy, Dan D.; Vijgen, Paul M.; Reimer, Heidi M.; Gallegos, Joey L.; and Spalart Philippe R.: "Recent NASA Wake-Vortex Flight Tests, Flow-Physics Database and Wake-Development Analysis," AIAA/SAE 1998 World Aviation Conference, AIAA/SAE 98-5592, September 1998.
2. Stuever, R. A.; Stewart, E. C.; and Rivers, R. A.: "Overview of the Preparation and Use of an OV-10 Aircraft for Wake Vortex Flight Experiments," AIAA 95-3935, September 1995.
3. Richardson, Norman R.: "Dynamic and Static Wind-Tunnel Tests of a Flow-Direction Vane," NASA TN D-6193, April 1971.
4. Taback, Isreal: "The Response of Pressure Measuring Systems to Oscillating Pressures," NACA TN-1819, February 1949.

5. Gracey, William: "Measurement of Aircraft Speed and Altitude," NASA RP-1046, May 1980.

Table 1. Data acquisition system recorded data parameters.

| Data # | Symbol | Database Name | Units | Sample Rate (Hz) | Description |
|--------|-------------------------|-------------------|----------|------------------|---|
| 0 | | <i>TIME</i> | seconds | 128 | Time |
| 1 | | <i>FWDVIB</i> | Gs | 128 | Nose boom vibrometer |
| 2 | | <i>LTVIB</i> | Gs | 128 | Left boom vibrometer |
| 3 | q_l' | <i>LT_AIRSP</i> | psi | 128 | Left boom raw dynamic pressure measurement |
| 4 | α_{Vn_l} | <i>LT_ALPHVN</i> | deg | 128 | Left boom raw angle of attack measurement |
| 5 | β_{Vn_l} | <i>LT_BETAVN</i> | deg | 128 | Left boom raw flank angle measurement |
| 6 | | <i>NSVIB</i> | Gs | 128 | Nose boom vibrometer |
| 7 | | <i>P3</i> | psi | 128 | Nose boom center hole pressure |
| 8 | $\Delta P_{3\alpha 1}'$ | <i>P3_PA1</i> | psi | 128 | Nose boom 5-hole probe pressure difference measurement |
| 9 | $\Delta P_{3\beta 1}'$ | <i>P3_PB1</i> | psi | 128 | Nose boom 5-hole probe pressure difference measurement |
| 10 | q_n' | <i>P3_PS</i> | psi | 128 | Nose boom dynamic pressure measurement |
| 11 | $\Delta P_{\alpha 12}'$ | <i>PA1_PA2</i> | psi | 128 | Nose boom angle of attack pressure difference measurement |
| 12 | $\Delta P_{\beta 12}'$ | <i>PB1_PB2</i> | psi | 128 | Nose boom sideslip angle pressure difference measurement |
| 13 | P_{s_n}' | <i>PS</i> | psi | 128 | Nose boom static pressure measurement |
| 14 | | <i>RTVIB</i> | Gs | 128 | Right boom vibrometer |
| 15 | q_r' | <i>RT_AIRSP</i> | psi | 128 | Right boom raw dynamic pressure measurement |
| 16 | α_{Vn_r} | <i>RT_ALPHVN</i> | deg | 128 | Right boom raw angle of attack measurement |
| 17 | β_{Vn_r} | <i>RT_BETAVN</i> | deg | 128 | Right boom raw flank angle measurement |
| 18 | | <i>TIMEDAYS</i> | days | 128 | Day |
| 19 | | <i>TIMEHRS</i> | hours | 128 | Hour |
| 20 | | <i>TIMEMIN</i> | minutes | 128 | Minute |
| 21 | | <i>TIMESEC</i> | seconds | 128 | Second |
| 22 | | <i>TIMEMILSEC</i> | millsecs | 128 | Millisecond |
| 23 | | <i>AIRTMP_ADC</i> | deg K | 8 | Outside air temperature from air-data computer |
| 24 | | <i>CAL_AS_ADC</i> | knots | 8 | Calibrated airspeed from air-data computer |
| 25 | | <i>DEWPTTEMP</i> | deg C | 32 | Dew-point temperature |

Table 1. Continued.

| Data # | Symbol | Database Name | Units | Sample Rate (Hz) | Description |
|--------|---------------|-------------------|----------|------------------|--|
| 26 | | <i>ELEVDEFL</i> | deg | 32 | Elevator deflection (+ trailing edge up) |
| 27 | | <i>EVENTMARK</i> | on / off | 32 | Event marker |
| 28 | \dot{E} | <i>E_W_VEL93</i> | ft/sec | 32 | Inertial velocity east from LN-93 INS |
| 29 | | <i>HEADING</i> | deg | 32 | True heading from mechanical gyro |
| 30 | | <i>INERTALT93</i> | ft | 32 | Inertial altitude from LN-93 INS |
| 31 | | <i>LATACC</i> | Gs | 32 | Lateral acceleration from accelerometer |
| 32 | | <i>LONGACC</i> | Gs | 32 | Longitudinal acceleration from accelerometer |
| 33 | | <i>LT_AILDEFL</i> | deg | 32 | Left aileron deflection (+ trailing edge up) |
| 34 | | <i>LT_PAL05</i> | psi | 32 | Left boom static pressure measurement (0 to 5000 ft) |
| 35 | | <i>LT_PAL510</i> | psi | 32 | Left boom static pressure measurement (5000 to 10000 ft) |
| 36 | P_{s_l}' | <i>LT_PRESAL</i> | psi | 32 | Left boom static pressure measurement (0 to 15000 ft) |
| 37 | | <i>LT_RUDDEFL</i> | deg | 32 | Left rudder deflection (+ trailing edge left) |
| 38 | | <i>MACHNO_ADC</i> | Mach | 8 | Mach number from air-data computer |
| 39 | | <i>NORMACC</i> | Gs | 32 | Normal acceleration from accelerometer |
| 40 | \dot{N} | <i>N_S_VEL93</i> | ft/sec | 32 | Inertial velocity north from LN-93 INS |
| 41 | T_m' | <i>OUTAIRTEMP</i> | deg C | 32 | Total-air-temperature from TAT probes |
| 42 | | <i>PITCHATT</i> | deg | 32 | Pitch angle from mechanical gyro |
| 43 | θ_{93} | <i>PITCHATT93</i> | deg | 32 | Pitch angle from LN-93 INS |
| 44 | q_m' | <i>PITCHRAT</i> | deg/sec | 32 | Pitch rate from mechanical gyro |
| 45 | | <i>PITCHRAT93</i> | deg/sec | 32 | Pitch rate from LN-93 INS |
| 46 | | <i>PLATAZ93</i> | deg | 32 | INS platform azimuth from LN-93 |
| 47 | | <i>PRESAL_ADC</i> | psi | 8 | Static pressure from air-data computer |
| 48 | | <i>ROLLATT</i> | deg | 32 | Roll angle from mechanical gyro |
| 49 | ϕ_{93} | <i>ROLLATT93</i> | deg | 32 | Roll angle from LN-93 INS |
| 50 | | <i>ROLLRATE93</i> | deg/sec | 32 | Roll rate from LN-93 INS |
| 51 | | <i>ROLLRATHI</i> | deg/sec | 32 | Roll rate from high range mechanical gyro |
| 52 | p_m' | <i>ROLLRATLOW</i> | deg/sec | 32 | Roll rate from low range mechanical gyro |
| 53 | | <i>RT_AILDEFL</i> | deg | 32 | Right aileron deflection (+ trailing edge down) |
| 54 | P_{s_r}' | <i>RT_PRESAL</i> | psi | 32 | Right boom static pressure measurement |
| 55 | | <i>TRUEAS_ADC</i> | knots | 8 | True airspeed from air-data computer |

Table 1. Concluded.

| Data # | Symbol | Database Name | Units | Sample Rate (Hz) | Description |
|--------|-------------|-------------------|-----------|------------------|--|
| 56 | | <i>TRUEAS_93</i> | knots | 32 | True airspeed from LN-93 INS |
| 57 | ψ_{93} | <i>TRUEHEAD93</i> | deg | 32 | True heading from LN-93 INS |
| 58 | \dot{z} | <i>VERTVEL93</i> | ft/sec | 32 | Inertial velocity up from LN-93 INS |
| 59 | r_m' | <i>YAWRAT</i> | deg/sec | 32 | Yaw rate from yaw gyro |
| 60 | | <i>YAWRATE93</i> | deg/sec | 32 | Yaw rate from LN-93 INS |
| 61 | | <i>XVEL93</i> | ft/sec | 32 | X inertial velocity from LN-93 INS in the navigation reference frame |
| 62 | | <i>YVEL93</i> | ft/sec | 32 | Y inertial velocity from LN-93 INS in the navigation reference frame |
| 63 | | <i>ZVEL93</i> | ft/sec | 32 | Z inertial velocity from LN-93 INS in the navigation reference frame |
| 64 | | <i>ALIGN_STAT</i> | 12 = done | | LN_93 alignment status flag |
| 65 | | <i>ALTDIFFGPS</i> | feet | 8 | |
| 66 | | <i>ALTGPS</i> | feet | 8 | Altitude from Honeywell GPS. Over-sampled, refreshed at 1/sec |
| 67 | | <i>CARGOTEMP1</i> | deg F | 8 | Cargo bay temperature |
| 68 | | <i>GARGOTEMP2</i> | deg F | 8 | Cargo bay temperature |
| 69 | | <i>CH1_CNR</i> | dB | 8 | Honeywell GPS channel 1 strength. Over-sampled, refreshed at 1/sec |
| 70 | | <i>CH2_CNR</i> | dB | 8 | Honeywell GPS channel 2 strength. Over-sampled, refreshed at 1/sec |
| 71 | | <i>CH3_CNR</i> | dB | 8 | Honeywell GPS channel 3 strength. Over-sampled, refreshed at 1/sec |
| 72 | | <i>CH4_CNR</i> | dB | 8 | Honeywell GPS channel 4 strength. Over-sampled, refreshed at 1/sec |
| 73 | | <i>CH5_CNR</i> | dB | 8 | Honeywell GPS channel 5 strength. Over-sampled, refreshed at 1/sec |
| 74 | | <i>CRVCR_MODE</i> | | 8 | Over-sampled, refreshed at 1/sec |
| 75 | | <i>DATAON</i> | on / off | 8 | Data switch position |
| 76 | | <i>DRIFTANG93</i> | deg | 8 | Drift angle from LN-93 INS |
| 116 | | <i>LAT93</i> | deg | 8 | Latitude from LN-93 INS Note: Over-sampled, refreshed at 4/sec |
| 117 | | <i>LATGPS</i> | deg | 8 | Latitude from Honeywell GPS. Over-sampled, refreshed at 1/sec |
| 118 | | <i>LONG93</i> | deg | 8 | Longitude from LN-93 INS Over-sampled, refreshed at 4/sec |
| 119 | | <i>LONGGPS</i> | deg | 8 | Longitude from Honeywell GPS. Over-sampled, refreshed at 1/sec |
| 120 | | <i>VELE_GPS</i> | ft/sec | 8 | Velocity east from Honeywell GPS. Over-sampled, refreshed at 1/sec |
| 121 | | <i>VELN_GPS</i> | ft/sec | 8 | Velocity north from Honeywell GPS. Over-sampled, refreshed at 1/sec |
| 122 | | <i>VELUP_GPS</i> | ft/sec | 8 | Velocity up from Honeywell GPS. Over-sampled, refreshed at 1/sec |

Table 2. Calibration coefficient values.

| Symbol | Default Value | Units | Description |
|---------------------------|---------------|---------|--|
| k_{α_r} | 0.8223 | - | Linear slope of right vane angle of attack calibration |
| k_{η_r} | 1.0073 | - | Linear slope of right flank angle vane calibration |
| k_{α_l} | 0.8363 | - | Linear slope of left vane angle of attack calibration |
| k_{η_l} | 0.9999 | - | Linear slope of left flank angle vane calibration |
| b_{α_r} | -1.7568 | deg | Calibration bias for right angle of attack vane |
| b_{η_r} | 1.4417 | deg | Calibration bias for right flank angle vane measurement |
| b_{α_l} | -0.8308 | deg | Calibration bias for left angle of attack vane |
| b_{η_l} | -0.1695 | deg | Calibration bias for left flank angle vane measurement |
| k_{α_n} | 0.8002 | - | Linear slope of the nose boom angle of attack calibration |
| k_{β_n} | 0.9183 | - | Linear slope of the nose boom side-slip calibration |
| b_{α_n} | 0.4420 | deg | Bias term of the nose boom angle of attack calibration |
| b_{β_n} | 0.5686 | deg | Bias term of the nose boom side-slip calibration |
| $k_{\Delta P_{qn}}$ | 0.08849 | - | Slope of nose boom position error correction curve for zero side-slip |
| $b_{\Delta P_{qn}}$ | -0.00752 | psi | Y-intercept of nose boom position error correction curve for zero side-slip |
| $k_{\Delta P_{qr}}$ | 0.014903 | - | Slope of right boom position error correction curve for zero side-slip |
| $b_{\Delta P_{qr}}$ | -0.00236 | psi | Y-intercept of right boom position error correction curve for zero side-slip |
| $k_{\Delta P_{ql}}$ | 0.018634 | - | Slope of left boom position error correction curve for zero side-slip |
| $b_{\Delta P_{ql}}$ | -0.00362 | psi | Y-intercept of left boom position error correction curve for zero side-slip |
| $k_{\Delta P_{q\beta_n}}$ | -0.00294 | psi/deg | Slope of nose boom position error correction due to side-slip |
| $k_{\Delta P_{q\beta_1}}$ | 0.000661 | psi/deg | Slope of wing boom position error correction due to side-slip |
| $k_{\Delta P_{q\beta_2}}$ | 0.000670 | psi/deg | Slope of wing boom position error correction due to side-slip |
| $b_{\Delta P_{q\beta_n}}$ | 0.010261 | psi | Y-intercept of nose boom position error correction curve due to side-slip |
| $b_{\Delta P_{q\beta_1}}$ | 0 | psi | Y-intercept of wing boom position error correction curve due to side-slip |
| $b_{\Delta P_{q\beta_2}}$ | 0 | psi | Y-intercept of wing boom position error correction curve due to side-slip |

Table 3. NACA pitot probe static pressure calibration coefficient (C_s) values.

| α , deg | $ \beta $, deg | | | | | | | | |
|----------------|-----------------|--------|--------|--------|--------|--------|--------|--------|--------|
| | 0 | 5 | 10 | 15 | 20 | 25 | 30 | 35 | 40 |
| -40 | 0.2976 | 0.3071 | 0.3245 | 0.3403 | 0.4263 | 0.5335 | 0.6680 | 0.6153 | 0.5247 |
| -38 | 0.2673 | 0.2761 | 0.2922 | 0.3088 | 0.3771 | 0.4839 | 0.6534 | 0.6481 | 0.5440 |
| -36 | 0.2482 | 0.2562 | 0.2709 | 0.2880 | 0.3407 | 0.4473 | 0.6194 | 0.6651 | 0.5635 |
| -34 | 0.2325 | 0.2405 | 0.2554 | 0.2729 | 0.3147 | 0.4121 | 0.5817 | 0.6648 | 0.5833 |
| -32 | 0.2158 | 0.2248 | 0.2411 | 0.2594 | 0.2963 | 0.3717 | 0.5456 | 0.6387 | 0.6027 |
| -30 | 0.1960 | 0.2067 | 0.2253 | 0.2453 | 0.2815 | 0.3360 | 0.4811 | 0.6077 | 0.6181 |
| -28 | 0.1763 | 0.1885 | 0.2127 | 0.2348 | 0.2723 | 0.3203 | 0.4270 | 0.5716 | 0.6262 |
| -26 | 0.1518 | 0.1648 | 0.1981 | 0.2221 | 0.2617 | 0.3104 | 0.3892 | 0.5455 | 0.6291 |
| -24 | 0.1308 | 0.1439 | 0.1785 | 0.2040 | 0.2458 | 0.2976 | 0.3600 | 0.5149 | 0.6252 |
| -22 | 0.1144 | 0.1272 | 0.1564 | 0.1843 | 0.2277 | 0.2827 | 0.3366 | 0.4814 | 0.6151 |
| -20 | 0.0942 | 0.1065 | 0.1372 | 0.1697 | 0.2151 | 0.2729 | 0.3235 | 0.4020 | 0.6006 |
| -18 | 0.0553 | 0.0673 | 0.1190 | 0.1599 | 0.2084 | 0.2685 | 0.3182 | 0.3646 | 0.5839 |
| -16 | 0.0366 | 0.0482 | 0.0975 | 0.1499 | 0.2014 | 0.2634 | 0.3127 | 0.3588 | 0.5676 |
| -14 | 0.0264 | 0.0378 | 0.0746 | 0.1348 | 0.1878 | 0.2513 | 0.3025 | 0.3493 | 0.5538 |
| -12 | 0.0195 | 0.0307 | 0.0619 | 0.1258 | 0.1791 | 0.2437 | 0.3005 | 0.3465 | 0.5424 |
| -10 | 0.0143 | 0.0252 | 0.0539 | 0.1190 | 0.1725 | 0.2375 | 0.3008 | 0.3479 | 0.5332 |
| -8 | 0.0097 | 0.0204 | 0.0495 | 0.1150 | 0.1688 | 0.2337 | 0.3012 | 0.3511 | 0.5258 |
| -6 | 0.0062 | 0.0167 | 0.0477 | 0.1130 | 0.1675 | 0.2318 | 0.3010 | 0.3544 | 0.5197 |
| -4 | 0.0033 | 0.0138 | 0.0467 | 0.1115 | 0.1666 | 0.2303 | 0.2995 | 0.3560 | 0.5148 |
| -2 | 0.0011 | 0.0117 | 0.0459 | 0.1101 | 0.1656 | 0.2287 | 0.2971 | 0.3554 | 0.5109 |
| 0 | 0.0000 | 0.0106 | 0.0452 | 0.1091 | 0.1648 | 0.2276 | 0.2949 | 0.3542 | 0.5081 |
| 2 | 0.0000 | 0.0108 | 0.0446 | 0.1083 | 0.1640 | 0.2269 | 0.2935 | 0.3536 | 0.5064 |
| 4 | 0.0000 | 0.0110 | 0.0431 | 0.1067 | 0.1624 | 0.2255 | 0.2919 | 0.3533 | 0.5058 |
| 6 | 0.0000 | 0.0112 | 0.0411 | 0.1047 | 0.1604 | 0.2240 | 0.2908 | 0.3545 | 0.5065 |
| 8 | 0.0011 | 0.0122 | 0.0412 | 0.1045 | 0.1603 | 0.2243 | 0.2919 | 0.3594 | 0.5085 |
| 10 | 0.0022 | 0.0124 | 0.0419 | 0.1043 | 0.1605 | 0.2238 | 0.2926 | 0.3652 | 0.5122 |
| 12 | 0.0040 | 0.0127 | 0.0437 | 0.1042 | 0.1611 | 0.2220 | 0.2924 | 0.3710 | 0.5183 |
| 14 | 0.0066 | 0.0145 | 0.0472 | 0.1046 | 0.1623 | 0.2217 | 0.2941 | 0.3789 | 0.5267 |
| 16 | 0.0098 | 0.0187 | 0.0528 | 0.1058 | 0.1644 | 0.2252 | 0.2998 | 0.3908 | 0.5350 |
| 18 | 0.0136 | 0.0243 | 0.0592 | 0.1083 | 0.1678 | 0.2307 | 0.3080 | 0.4044 | 0.5408 |
| 20 | 0.0182 | 0.0302 | 0.0655 | 0.1126 | 0.1727 | 0.2364 | 0.3166 | 0.4173 | 0.5447 |
| 22 | 0.0236 | 0.0362 | 0.0716 | 0.1182 | 0.1788 | 0.2415 | 0.3254 | 0.4284 | 0.5476 |
| 24 | 0.0290 | 0.0421 | 0.0772 | 0.1240 | 0.1848 | 0.2457 | 0.3337 | 0.4369 | 0.5507 |
| 26 | 0.0337 | 0.0472 | 0.0819 | 0.1292 | 0.1901 | 0.2499 | 0.3421 | 0.4443 | 0.5552 |
| 28 | 0.0379 | 0.0514 | 0.0857 | 0.1340 | 0.1948 | 0.2560 | 0.3516 | 0.4531 | 0.5607 |
| 30 | 0.0421 | 0.0549 | 0.0888 | 0.1383 | 0.1989 | 0.2652 | 0.3629 | 0.4581 | 0.5608 |
| 32 | 0.0454 | 0.0566 | 0.0901 | 0.1412 | 0.2017 | 0.2750 | 0.3738 | 0.4665 | 0.5506 |
| 34 | 0.0471 | 0.0565 | 0.0897 | 0.1428 | 0.2031 | 0.2836 | 0.3828 | 0.4821 | 0.5355 |
| 36 | 0.0478 | 0.0563 | 0.0895 | 0.1447 | 0.2049 | 0.2910 | 0.3903 | 0.4829 | 0.5221 |
| 38 | 0.0482 | 0.0574 | 0.0908 | 0.1482 | 0.2085 | 0.2990 | 0.3986 | 0.4757 | 0.5109 |
| 40 | 0.0489 | 0.0598 | 0.0934 | 0.1534 | 0.2138 | 0.3088 | 0.4084 | 0.4583 | 0.5007 |

Table 4. NACA pitot probe dynamic pressure calibration coefficient (C_q) values.

| α , deg | $ \beta $, deg | | | | | | | | |
|----------------|-----------------|---------|---------|---------|---------|---------|---------|---------|---------|
| | 0 | 5 | 10 | 15 | 20 | 25 | 30 | 35 | 40 |
| -40 | 0.0440 | 0.0473 | 0.0489 | 0.0604 | 0.0366 | 0.0147 | -0.0159 | 0.1368 | 0.3529 |
| -38 | 0.0129 | 0.0118 | 0.0148 | 0.0249 | 0.0118 | -0.0108 | -0.0764 | 0.0299 | 0.2597 |
| -36 | -0.0183 | -0.0201 | -0.0160 | -0.0068 | -0.0110 | -0.0358 | -0.1039 | -0.0473 | 0.1799 |
| -34 | -0.0477 | -0.0507 | -0.0475 | -0.0391 | -0.0381 | -0.0587 | -0.1242 | -0.1038 | 0.1032 |
| -32 | -0.0705 | -0.0755 | -0.0749 | -0.0676 | -0.0663 | -0.0728 | -0.1432 | -0.1308 | 0.0300 |
| -30 | -0.0835 | -0.0911 | -0.0946 | -0.0894 | -0.0907 | -0.0857 | -0.1302 | -0.1485 | -0.0351 |
| -28 | -0.0937 | -0.1034 | -0.1144 | -0.1127 | -0.1174 | -0.1143 | -0.1280 | -0.1614 | -0.0936 |
| -26 | -0.0911 | -0.1021 | -0.1242 | -0.1269 | -0.1356 | -0.1387 | -0.1372 | -0.1806 | -0.1424 |
| -24 | -0.0851 | -0.0966 | -0.1219 | -0.1299 | -0.1430 | -0.1525 | -0.1462 | -0.1894 | -0.1776 |
| -22 | -0.0804 | -0.0919 | -0.1133 | -0.1289 | -0.1466 | -0.1615 | -0.1560 | -0.1948 | -0.2043 |
| -20 | -0.0690 | -0.0803 | -0.1044 | -0.1282 | -0.1520 | -0.1719 | -0.1698 | -0.1549 | -0.2238 |
| -18 | -0.0366 | -0.0478 | -0.0940 | -0.1275 | -0.1587 | -0.1840 | -0.1859 | -0.1558 | -0.2389 |
| -16 | -0.0230 | -0.0340 | -0.0787 | -0.1247 | -0.1623 | -0.1934 | -0.1983 | -0.1752 | -0.2505 |
| -14 | -0.0169 | -0.0277 | -0.0606 | -0.1154 | -0.1573 | -0.1938 | -0.2034 | -0.1822 | -0.2583 |
| -12 | -0.0130 | -0.0239 | -0.0519 | -0.1113 | -0.1557 | -0.1968 | -0.2149 | -0.1949 | -0.2674 |
| -10 | -0.0101 | -0.0207 | -0.0468 | -0.1082 | -0.1546 | -0.1989 | -0.2262 | -0.2106 | -0.2773 |
| -8 | -0.0071 | -0.0177 | -0.0447 | -0.1070 | -0.1551 | -0.2015 | -0.2356 | -0.2263 | -0.2866 |
| -6 | -0.0048 | -0.0152 | -0.0446 | -0.1070 | -0.1568 | -0.2044 | -0.2428 | -0.2401 | -0.2947 |
| -4 | -0.0026 | -0.0129 | -0.0445 | -0.1068 | -0.1578 | -0.2063 | -0.2471 | -0.2502 | -0.3014 |
| -2 | -0.0008 | -0.0112 | -0.0443 | -0.1064 | -0.1582 | -0.2074 | -0.2495 | -0.2566 | -0.3069 |
| 0 | 0.0000 | -0.0104 | -0.0441 | -0.1060 | -0.1582 | -0.2086 | -0.2515 | -0.2612 | -0.3117 |
| 2 | 0.0000 | -0.0106 | -0.0436 | -0.1053 | -0.1576 | -0.2094 | -0.2532 | -0.2647 | -0.3154 |
| 4 | 0.0000 | -0.0108 | -0.0421 | -0.1036 | -0.1559 | -0.2092 | -0.2539 | -0.2671 | -0.3184 |
| 6 | 0.0000 | -0.0110 | -0.0402 | -0.1016 | -0.1538 | -0.2086 | -0.2541 | -0.2695 | -0.3208 |
| 8 | -0.0011 | -0.0120 | -0.0402 | -0.1014 | -0.1537 | -0.2093 | -0.2556 | -0.2741 | -0.3227 |
| 10 | -0.0021 | -0.0122 | -0.0409 | -0.1012 | -0.1538 | -0.2087 | -0.2558 | -0.2780 | -0.3247 |
| 12 | -0.0038 | -0.0124 | -0.0426 | -0.1011 | -0.1542 | -0.2062 | -0.2539 | -0.2802 | -0.3271 |
| 14 | -0.0063 | -0.0140 | -0.0460 | -0.1014 | -0.1551 | -0.2046 | -0.2528 | -0.2828 | -0.3299 |
| 16 | -0.0092 | -0.0180 | -0.0512 | -0.1022 | -0.1564 | -0.2061 | -0.2548 | -0.2877 | -0.3307 |
| 18 | -0.0127 | -0.0233 | -0.0573 | -0.1040 | -0.1586 | -0.2093 | -0.2582 | -0.2928 | -0.3273 |
| 20 | -0.0170 | -0.0288 | -0.0630 | -0.1072 | -0.1617 | -0.2119 | -0.2607 | -0.2955 | -0.3201 |
| 22 | -0.0220 | -0.0344 | -0.0684 | -0.1114 | -0.1653 | -0.2129 | -0.2617 | -0.2947 | -0.3100 |
| 24 | -0.0268 | -0.0396 | -0.0730 | -0.1152 | -0.1678 | -0.2116 | -0.2601 | -0.2896 | -0.2982 |
| 26 | -0.0305 | -0.0437 | -0.0762 | -0.1178 | -0.1686 | -0.2083 | -0.2561 | -0.2814 | -0.2856 |
| 28 | -0.0332 | -0.0464 | -0.0778 | -0.1191 | -0.1674 | -0.2037 | -0.2499 | -0.2717 | -0.2710 |
| 30 | -0.0349 | -0.0473 | -0.0773 | -0.1186 | -0.1636 | -0.1981 | -0.2415 | -0.2546 | -0.2472 |
| 32 | -0.0339 | -0.0444 | -0.0729 | -0.1142 | -0.1551 | -0.1899 | -0.2299 | -0.2381 | -0.2101 |
| 34 | -0.0298 | -0.0380 | -0.0650 | -0.1048 | -0.1404 | -0.1778 | -0.2144 | -0.2269 | -0.1661 |
| 36 | -0.0224 | -0.0289 | -0.0544 | -0.0925 | -0.1217 | -0.1619 | -0.1959 | -0.1992 | -0.1221 |
| 38 | -0.0104 | -0.0161 | -0.0402 | -0.0772 | -0.1016 | -0.1441 | -0.1768 | -0.1622 | -0.0788 |
| 40 | 0.0086 | 0.0030 | -0.0198 | -0.0561 | -0.0775 | -0.1222 | -0.1541 | -0.1098 | -0.0315 |

Table 5. Airplane axis coordinates of system components.

| x , ft | y , ft | z , ft | Description |
|----------|----------|----------|--------------------------------------|
| -6.3675 | 19.7242 | -2.6875 | right boom |
| -6.3658 | -19.7242 | -2.6875 | left boom tip |
| 5.6108 | 2.1308 | 0.6292 | nose boom tip |
| -14.5833 | 1.2083 | 0.5779 | body axis origin (x_b, y_b, z_b) |

Table 6. OVDRA calculated and recorded parameters.

| Symbol | Units | Eqn # | Description |
|--------------|--------|-------|--|
| α_r | deg | 22 | Right boom local angle of attack |
| α_l | deg | 23 | Left boom local angle of attack |
| α_n | deg | 24 | Nose boom local angle of attack |
| η_r | deg | 25 | Right boom flank angle |
| η_l | deg | 26 | Left boom flank angle |
| β_n | deg | 28 | Nose boom local sideslip angle |
| q_r | psi | 38 | Right boom dynamic pressure |
| q_l | psi | 38 | Left boom dynamic pressure |
| q_n | psi | 39 | Nose boom dynamic pressure |
| Ps_r | psi | 36 | Right boom static pressure |
| Ps_l | psi | 36 | Left boom static pressure |
| Ps_n | psi | 37 | Nose boom static pressure |
| M_r | - | 40 | Right boom local Mach number |
| M_l | - | 40 | Left boom local Mach number |
| M_n | - | 40 | Nose boom local Mach number |
| T_{abs} | °R | 42 | Local absolute temperature |
| T_∞ | °R | 43 | Local free-stream air temperature |
| T_θ | °R | 44 | Potential temperature |
| a | ft/sec | 45 | Local speed of sound |
| Vt_{loc_r} | ft/sec | 46 | Right boom local true airspeed |
| Vt_{loc_l} | ft/sec | 46 | Left boom local true airspeed |
| Vt_{loc_n} | ft/sec | 46 | Nose boom local true airspeed |
| β_r | deg | 27 | Right boom local sideslip angle |
| β_l | deg | 27 | Left boom local sideslip angle |
| u_{b_r} | ft/sec | 47 | Right boom body axis longitudinal airspeed |
| u_{b_l} | ft/sec | 47 | Left boom body axis longitudinal airspeed |
| u_{b_n} | ft/sec | 47 | Nose boom body axis longitudinal airspeed |

Table 6. Continued.

| Symbol | Units | Eqn # | Description |
|------------------------|--------|-------|--|
| v_{b_r} | ft/sec | 48 | Right boom body axis lateral airspeed |
| v_{b_l} | ft/sec | 48 | Left boom body axis lateral airspeed |
| v_{b_n} | ft/sec | 48 | Nose boom body axis lateral airspeed |
| w_{b_r} | ft/sec | 49 | Right boom body axis vertical airspeed |
| w_{b_l} | ft/sec | 49 | Left boom body axis vertical airspeed |
| w_{b_n} | ft/sec | 49 | Nose boom body axis vertical airspeed |
| Vt_r | ft/sec | 50 | Right boom true airspeed |
| Vt_l | ft/sec | 50 | Left boom true airspeed |
| Vt_n | ft/sec | 50 | Nose boom true airspeed |
| α_{t_r} | deg | 51 | Right boom angle of attack |
| α_{t_l} | deg | 51 | Left boom angle of attack |
| α_{t_n} | deg | 51 | Nose boom angle of attack |
| β_{t_r} | deg | 52 | Right boom sideslip angle |
| β_{t_l} | deg | 52 | Left boom sideslip angle |
| β_{t_n} | deg | 52 | Nose boom sideslip angle |
| Vt_{avg} | ft/sec | 53 | Average true airspeed |
| $u_{b_{avg}}$ | ft/sec | 54 | Average body axis longitudinal airspeed |
| $v_{b_{avg}}$ | ft/sec | 55 | Average body axis lateral airspeed |
| $w_{b_{avg}}$ | ft/sec | 56 | Average body axis vertical airspeed |
| α_{avg} | deg | 57 | Average angle of attack |
| β_{avg} | deg | 58 | Average sideslip angle |
| $\mathbf{T}_{be}(1,1)$ | - | 60 | Body to Earth axis transformation matrix element |
| $\mathbf{T}_{be}(1,2)$ | - | 60 | Body to Earth axis transformation matrix element |
| $\mathbf{T}_{be}(1,3)$ | - | 60 | Body to Earth axis transformation matrix element |
| $\mathbf{T}_{be}(2,1)$ | - | 60 | Body to Earth axis transformation matrix element |
| $\mathbf{T}_{be}(2,2)$ | - | 60 | Body to Earth axis transformation matrix element |
| $\mathbf{T}_{be}(2,3)$ | - | 60 | Body to Earth axis transformation matrix element |
| $\mathbf{T}_{be}(3,1)$ | - | 60 | Body to Earth axis transformation matrix element |
| $\mathbf{T}_{be}(3,2)$ | - | 60 | Body to Earth axis transformation matrix element |
| $\mathbf{T}_{be}(3,3)$ | - | 60 | Body to Earth axis transformation matrix element |
| W_{Nr} | ft/sec | 61 | Right boom northerly wind velocity |
| W_{Er} | ft/sec | 62 | Right boom easterly wind velocity |
| W_{Zr} | ft/sec | 63 | Right boom vertical wind velocity |

Table 6. Concluded.

| Symbol | Units | Eqn # | Description |
|--------------|--------|-------|--|
| W_{Nl} | ft/sec | 61 | Left boom northerly wind velocity |
| W_{El} | ft/sec | 62 | Left boom easterly wind velocity |
| W_{Zl} | ft/sec | 63 | Left boom vertical wind velocity |
| W_{Nn} | ft/sec | 61 | Nose boom northerly wind velocity |
| W_{En} | ft/sec | 62 | Nose boom easterly wind velocity |
| W_{Zn} | ft/sec | 63 | Nose boom vertical wind velocity |
| W_{Navg} | ft/sec | 61 | Average northerly wind velocity |
| W_{Eavg} | ft/sec | 62 | Average easterly wind velocity |
| W_{Zavg} | ft/sec | 63 | Average vertical wind velocity |
| V_{wnd} | knots | 66 | Average wind speed |
| Ψ_{wnd} | deg | 67 | Average wind direction in degrees true |

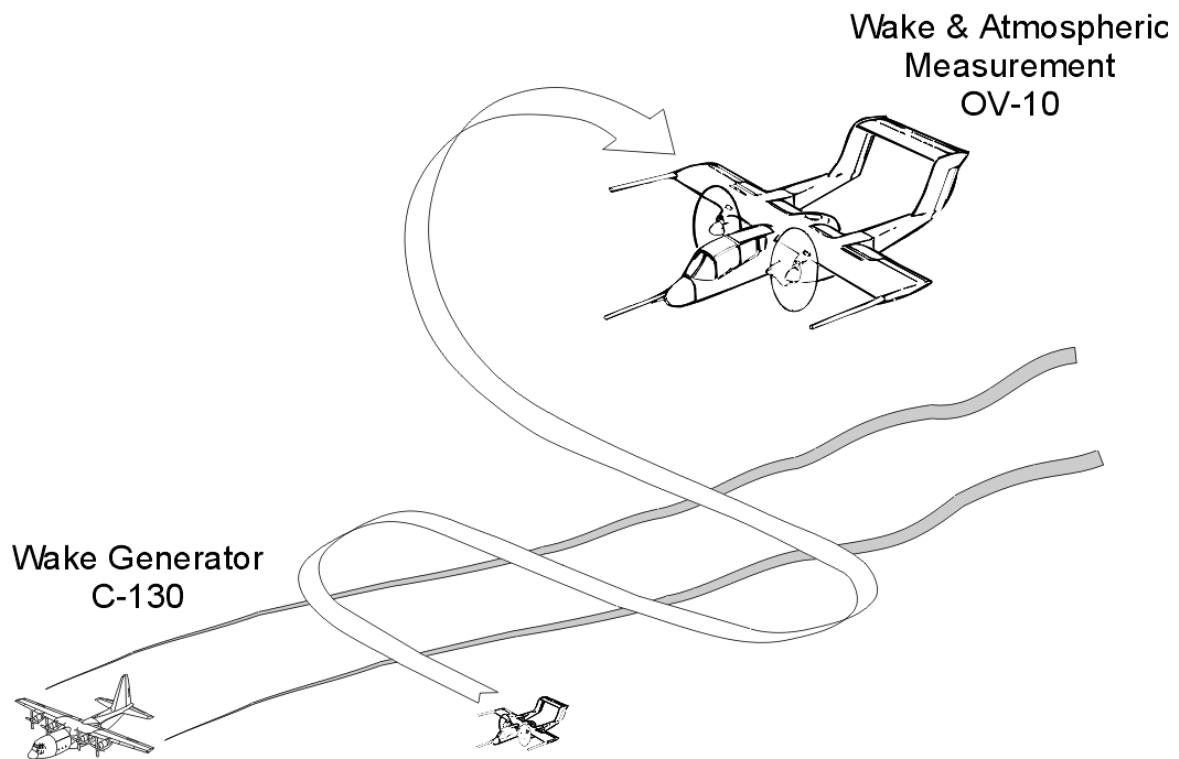


Figure 1. - Wake measurement flight test setup.



Figure 2. - C-130 wake generator airplane.

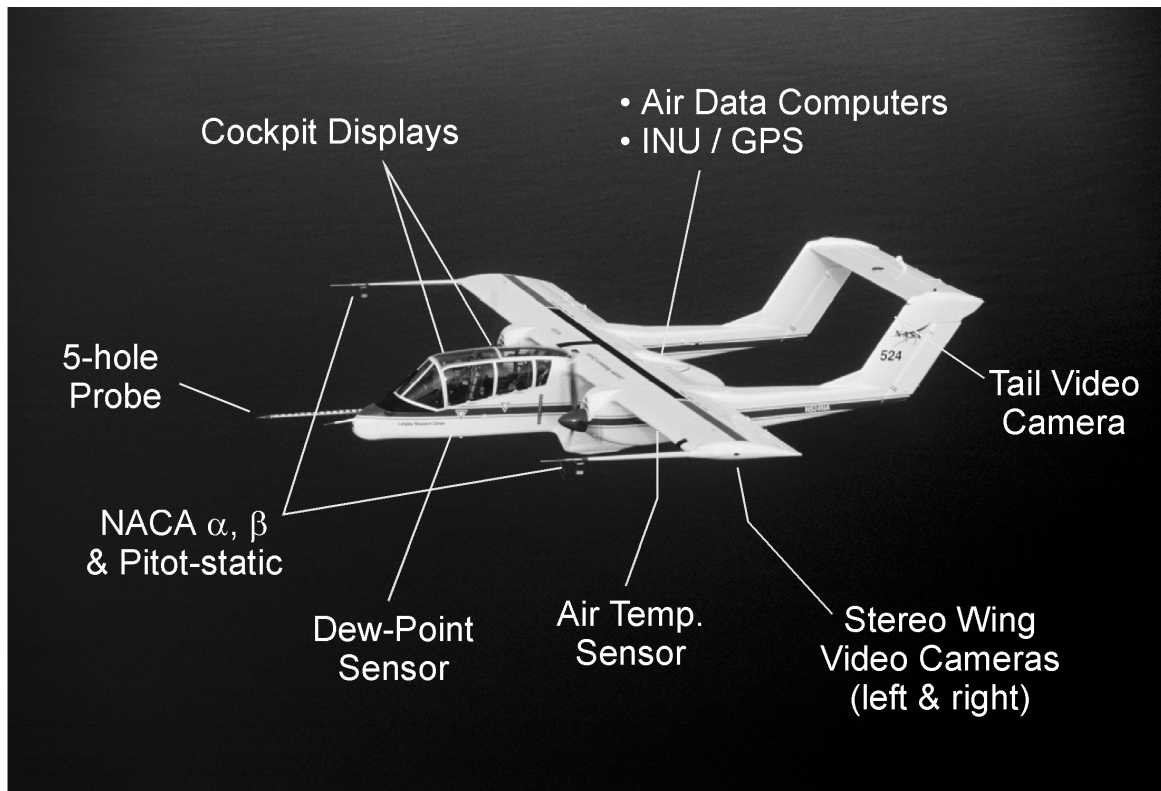


Figure 3. - OV-10 major instrumentation systems

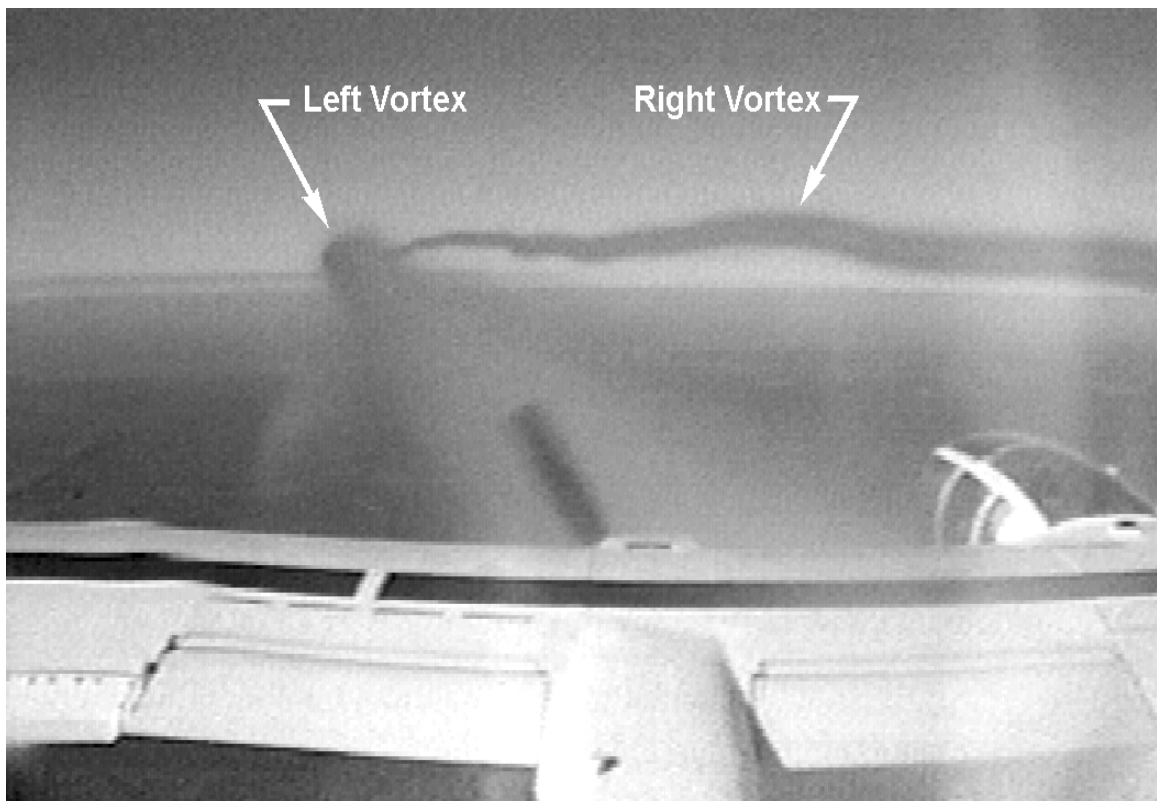
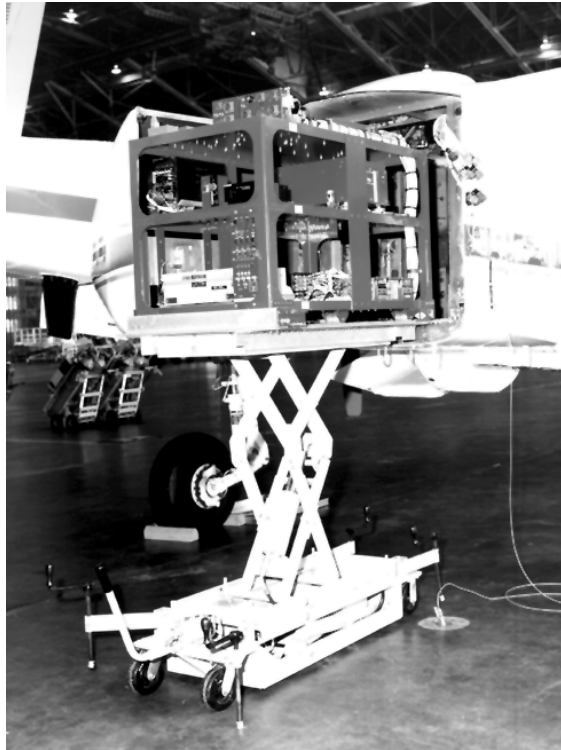
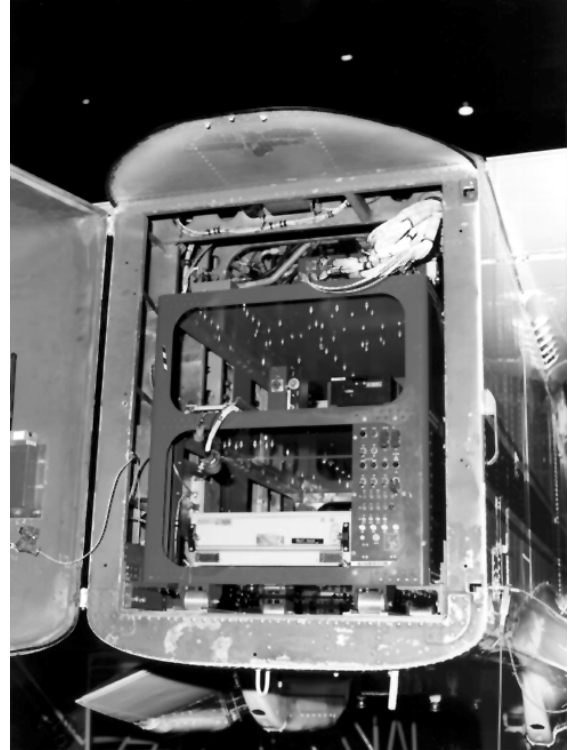


Figure 4. - OV-10 tail video of wake measurement.



(a) Pallet outside of cargo bay.



(b) Pallet installed for flight.

Figure 5. – Data acquisition system research pallet.

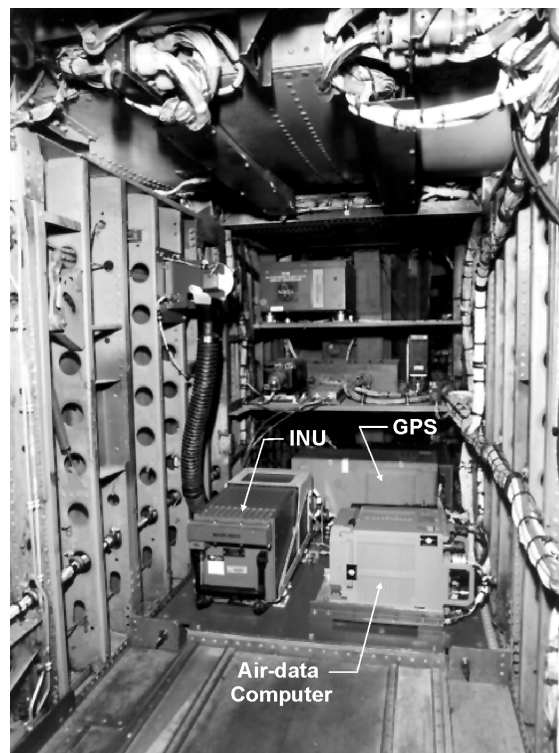


Figure 6. – Research equipment in the forward cargo-bay area.

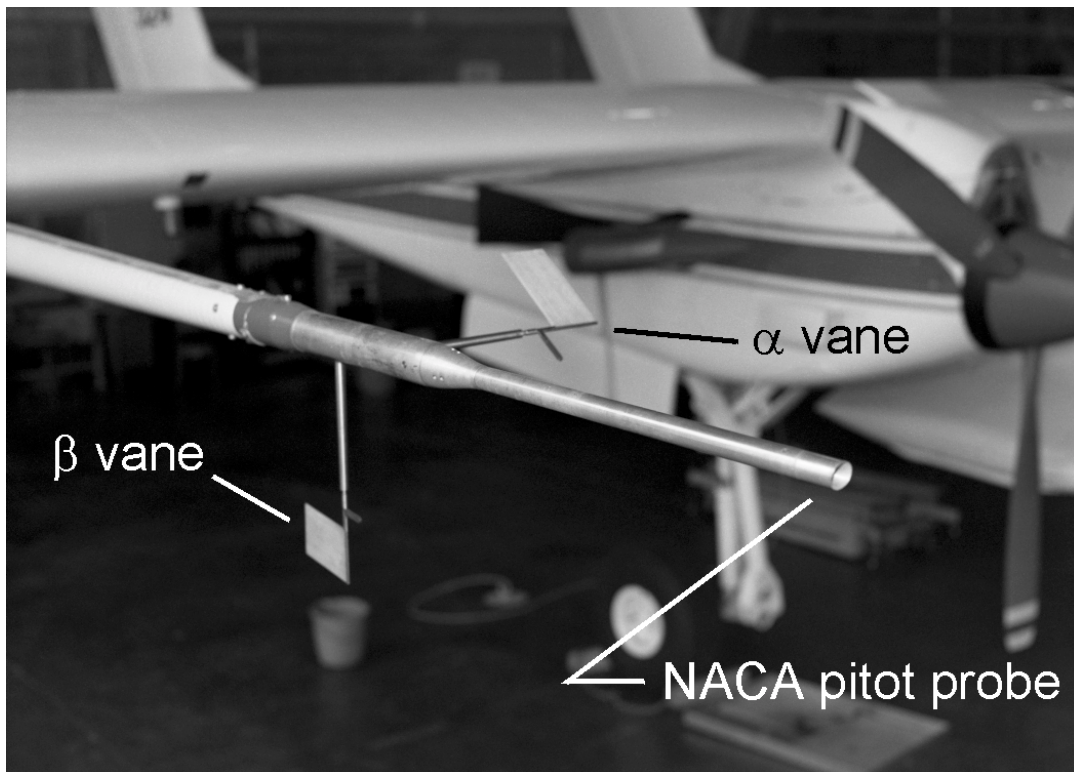


Figure 7. – Right boom NACA pitot probe with angle of attack and sideslip vanes.

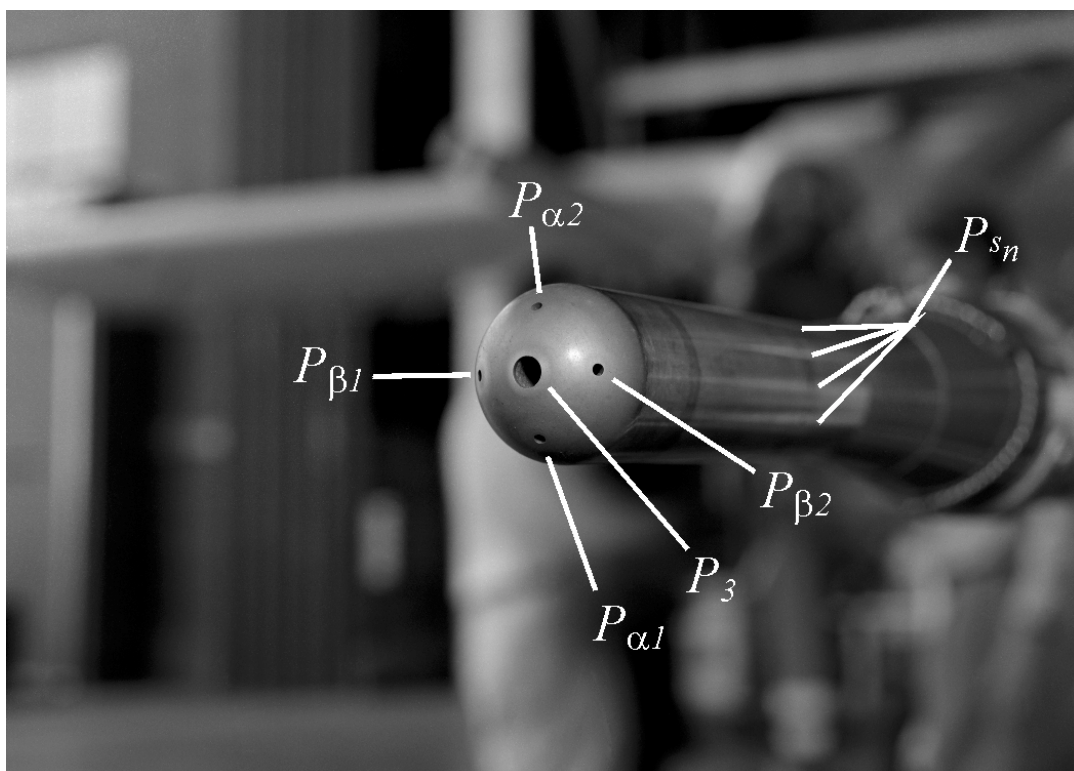


Figure 8. – Nose boom 5-hole probe.

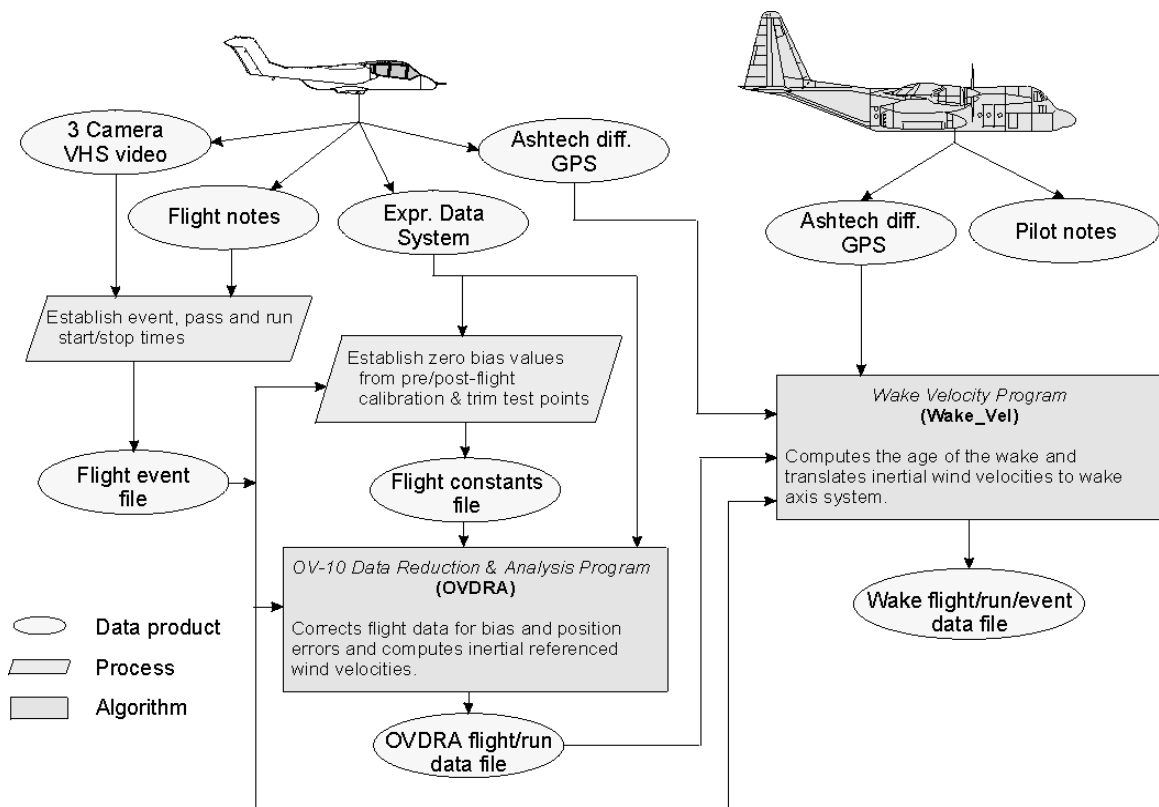


Figure 9. – Flight data reduction process.

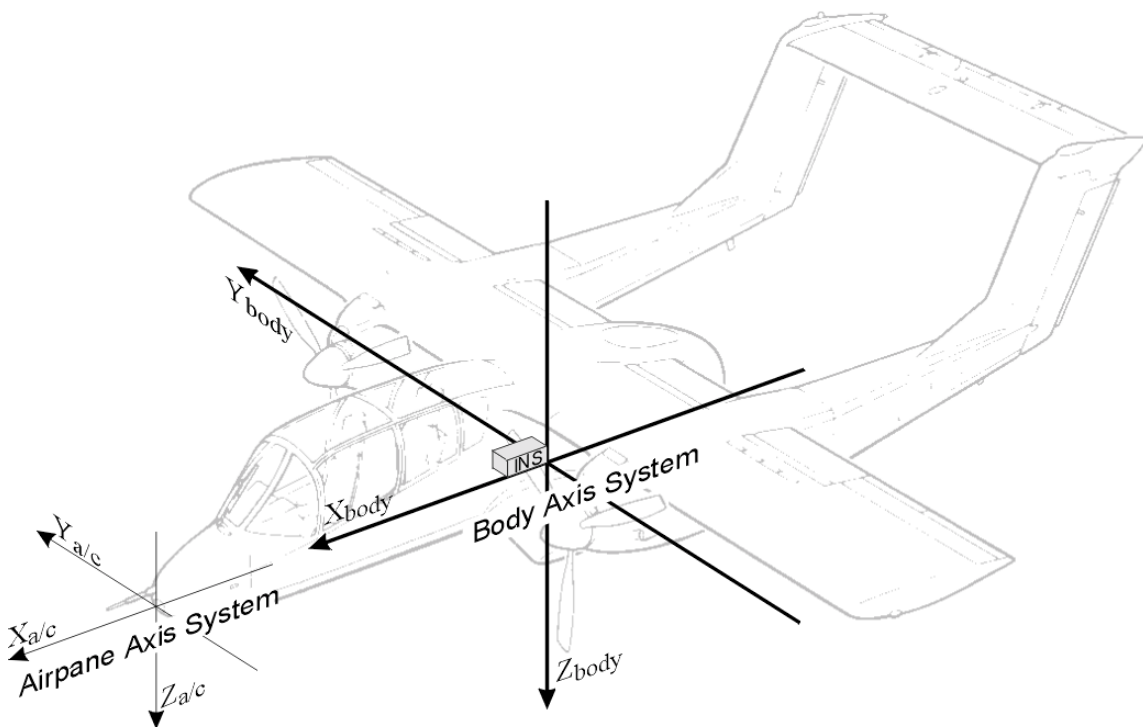


Figure 10. – Airplane and body axis systems.

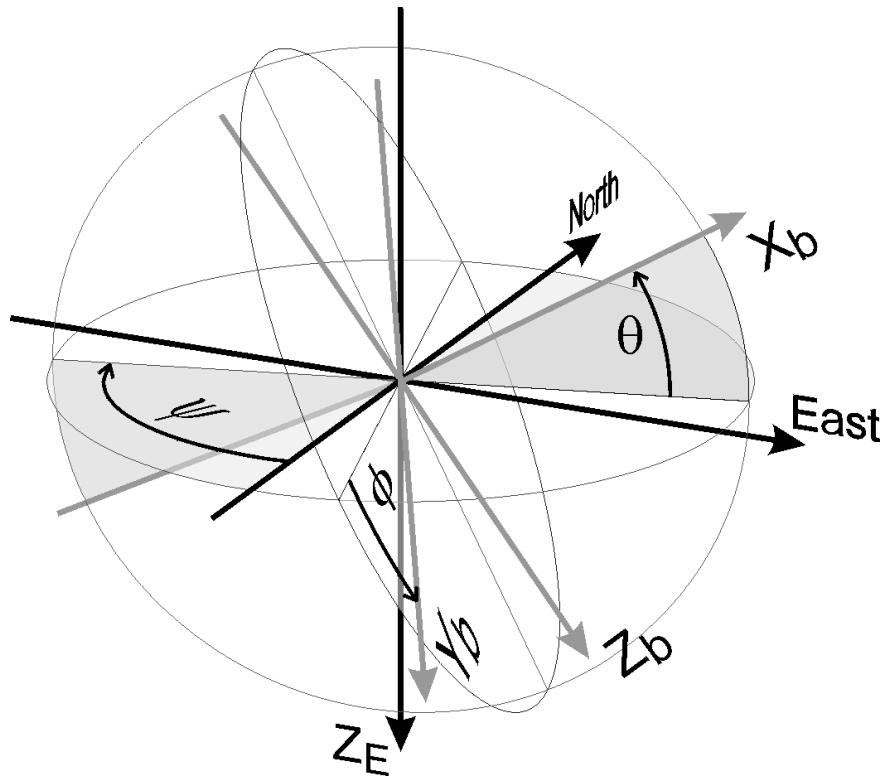


Figure 11. – Euler angles with body and inertial axis systems.

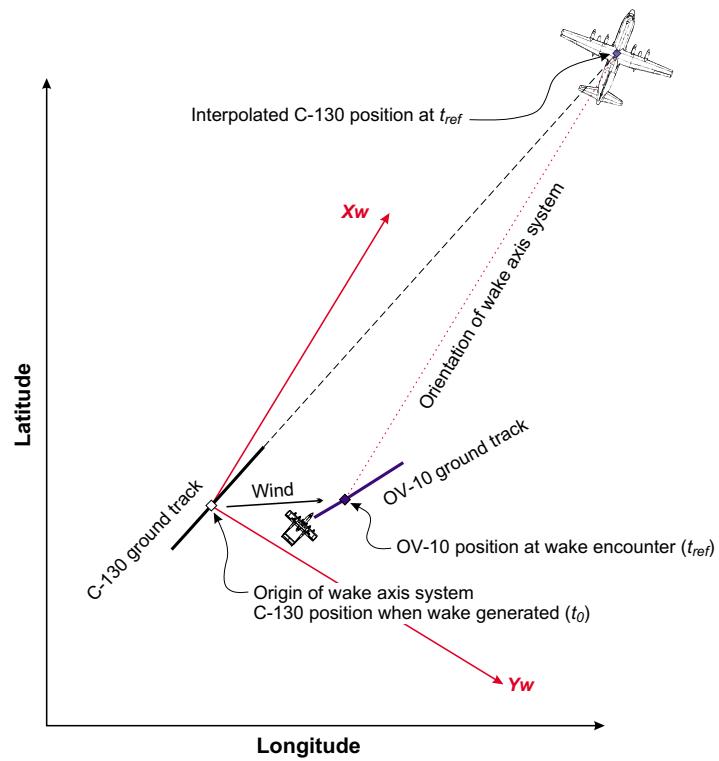


Figure 12. - Wake axis system

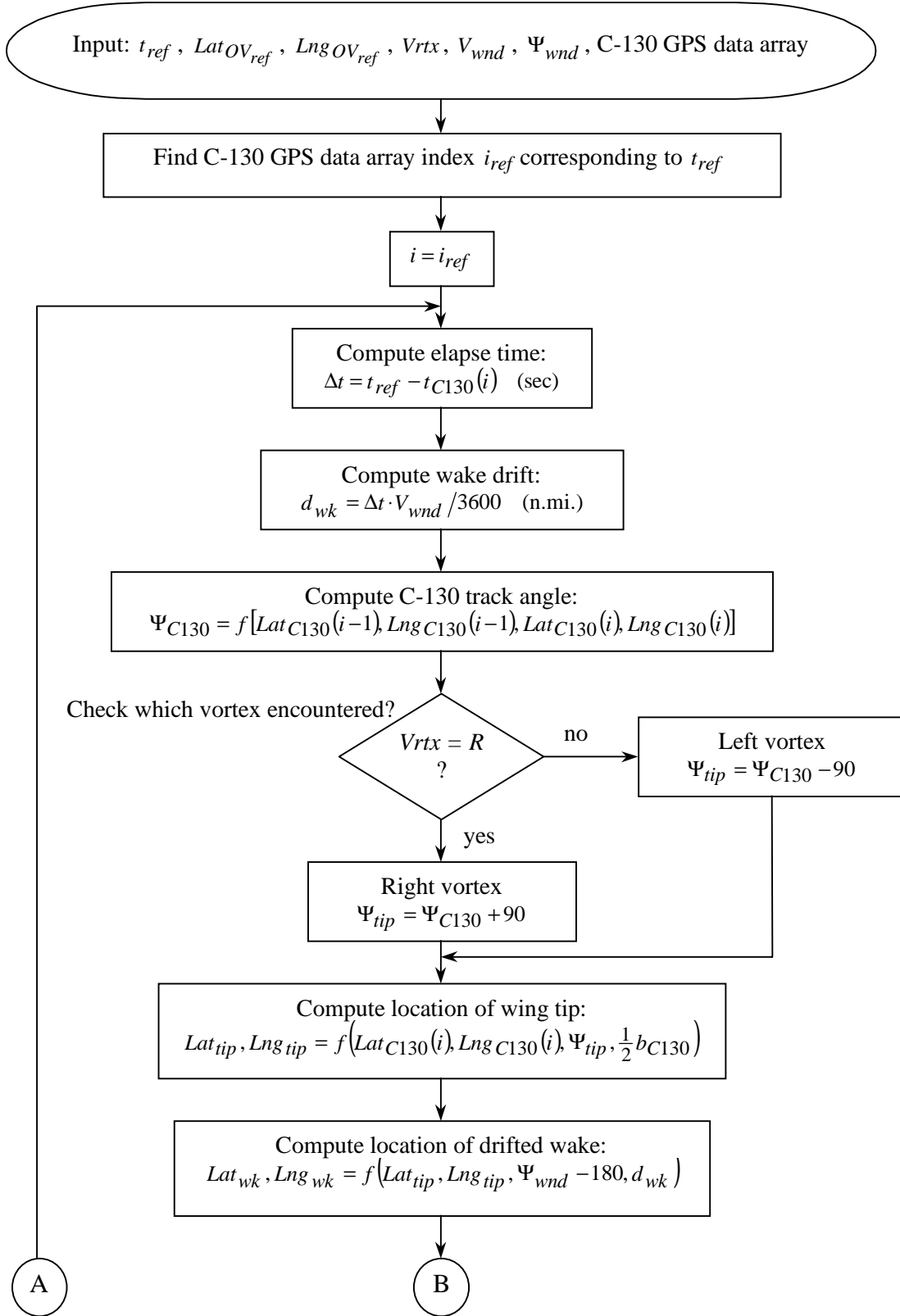


Figure 13. Flowchart of wake origin calculation.

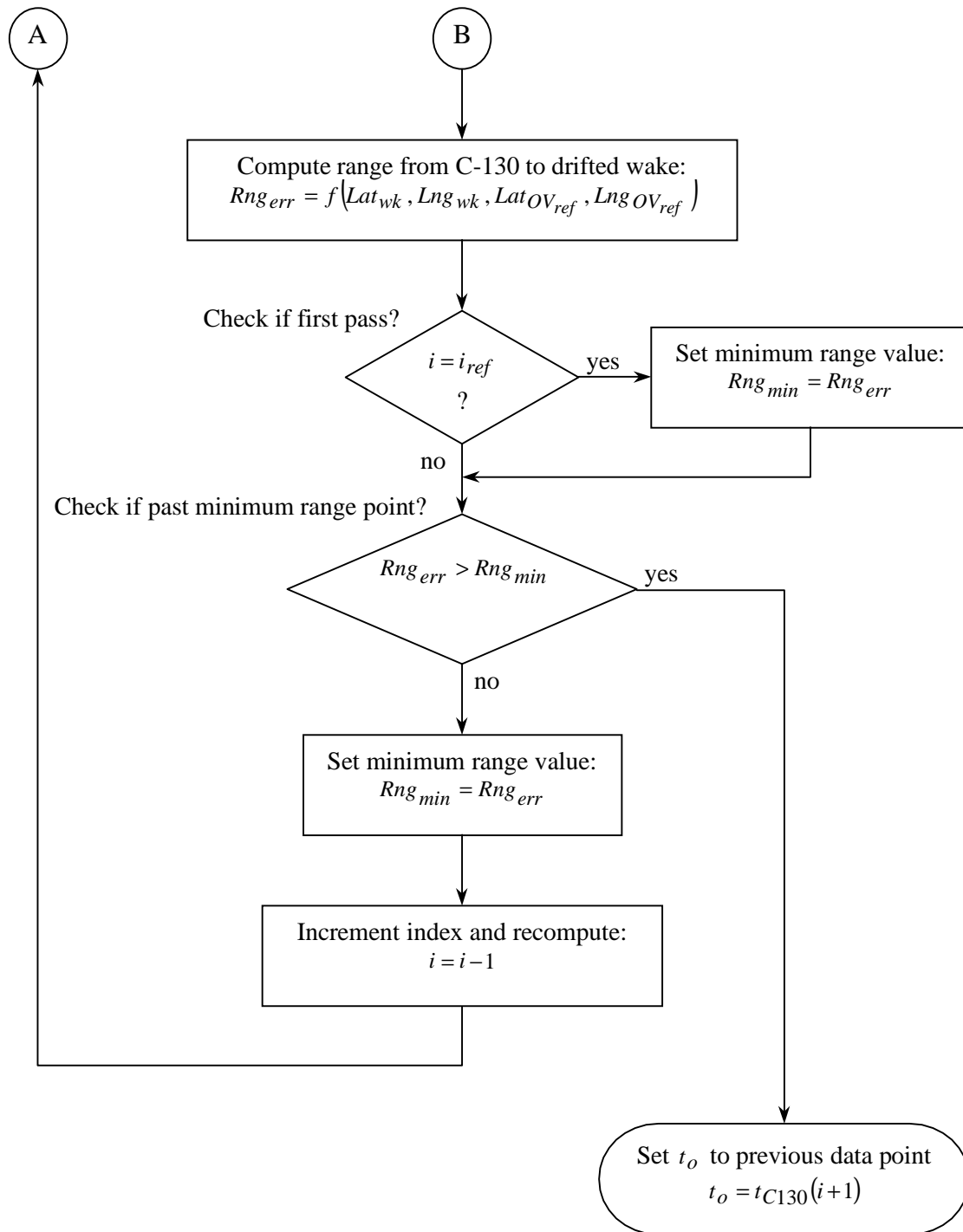


Figure 13. Concluded.

Appendix A – OV-10 Airspeed Calibration

The objective of the OV-10 airspeed calibration was to determine the position-error pressure corrections and the angle-of-attack and sideslip calibration for the three booms. The airspeed calibration flights were Flight 613 flown on September 24, 1996 and Flight 614 flown on November 13, 1996. The position error corrections for the left, right and nose boom were computed in a similar manner as the “camera method” described in reference 5. The difference between the method outlined here and the camera method was that the airplane altitude was determined from differential GPS measurements rather than photographically.

Flight Test Procedure

The basic test procedure involved flying a series of steady, low altitude, level passes at different airspeeds and sideslip angles. A row of 140-foot tall light towers at Langley Airforce Base (LAFB) served as a visual reference for the level passes. After every two or three low altitude passes the OV-10 would land and collect static surface data such as temperature, pressure and wind measurements. Pre- and post-flight instrument calibration data and in-flight steady trim data were also collected to determine instrumentation bias values. The data from the OV-10 experimental data system was reduced from 128 Hz to 1 Hz using a one-second-averaging interval.

Computing Reference Values

The first step in determining the calibration corrections is to compute the reference values from which the measured values are calibrated. This basically involves extrapolating surface measurements to the pass altitude based on a measured lapse rate.

Reference Angle of Attack and Sideslip Calculation

The wind velocity components during the pass must be determined to compute the reference sideslip and angle of attack. The LAFB surface winds, which were measured 12 feet above the runway, were recorded throughout each flight. Figure A1 shows the surface wind time history for both flights. The numerous takeoffs and landings throughout the flight provided a time history of the wind change with altitude. The change in the wind speed and direction with altitude was computed for each takeoff and landing through a linear fit of the measured winds from 8 to 16 feet and from 120 to 160 feet above the runway. The assumption here is that although the magnitude of OV-10 wind velocity and direction measurements were not yet calibrated and therefore not valid, the measured change of the wind velocity and direction were essentially correct. The time histories of the computed wind gradients for both flights are shown in figure A2.

The reference wind speed and direction for a given pass was computed through a linear interpolation of the surface wind speed and direction and the altitude-gradients as a function of the pass time and altitude. The altitudes were determined from the differential Ashtech GPS measurements.

$$V_{wnd}(t_{pass}) = \frac{dV_{wnd}}{dh}(t_{pass}) \cdot (h_{pass} - h_{grnd}) + V_{wnd_{grnd}}(t_{pass}) \quad (\text{knots}) \quad (\text{A1})$$

$$\Psi_{wnd}(t_{pass}) = \frac{d\Psi_{wnd}}{dh}(t_{pass}) \cdot (h_{pass} - h_{grnd}) + \Psi_{wnd_{grnd}}(t_{pass}) \quad (\text{deg. magnetic}) \quad (\text{A2})$$

The inertial wind components are computed from the wind direction and speed through:

$$W_N = -1.688 V_{wnd} \cos\left(\Psi_{wnd_{mag}} - Mag_{var}\right) \quad (\text{fps}) \quad (\text{A3})$$

$$W_E = -1.688 V_{wnd} \sin\left(\Psi_{wnd_{mag}} - Mag_{var}\right) \quad (\text{fps}) \quad (\text{A4})$$

$$W_Z = 0 \quad (\text{fps}) \quad (\text{A5})$$

where the magnetic variation (Mag_{var}) at the test site was 9.23 degrees west.

The reference true airspeed was computed as:

$$V_{t_{ref}} = \sqrt{(\dot{N} - W_N)^2 + (\dot{E} - W_E)^2 + (-\dot{Z} - W_Z)^2} \quad (\text{fps}) \quad (\text{A6})$$

The air-mass-relative body-axis velocity components were computed from:

$$\begin{pmatrix} u_{b_{ref}} \\ v_{b_{ref}} \\ w_{b_{ref}} \end{pmatrix} = \mathbf{T}_{be}^{-1} \begin{pmatrix} \dot{N} - W_N \\ \dot{E} - W_E \\ -\dot{Z} - W_Z \end{pmatrix} \quad (\text{fps}) \quad (\text{A7})$$

where \mathbf{T}_{be} is defined in equation 60.

The reference angle of attack was computed as:

$$\alpha_{ref} = \tan^{-1} \left(\frac{w_{b_{ref}}}{u_{b_{ref}}} \right) \quad (\text{deg}) \quad (\text{A8})$$

and the reference sideslip from:

$$\beta_{ref} = \sin^{-1} \left(\frac{v_{b_{ref}}}{V_{t_{ref}}} \right) \quad (\text{deg}) \quad (\text{A9})$$

The wing boom balsa vanes measure the flank angle rather than the sideslip angle. The reference flank angle was computed as:

$$\eta_{ref} = \tan^{-1} \left(\frac{\tan \beta_{ref}}{\cos \alpha_{ref}} \right) \quad (\text{deg}) \quad (\text{A10})$$

Reference Static Pressure Calculation

The reference static pressure was determined by extrapolating the surface measurements to the probe altitude assuming a standard density lapse rate. Time histories of the ground static pressure and temperature measurements from the OV-10 are shown in figures A3 and A4, respectively. Also shown in figure A3 are the static pressure measurements from an independent ground measurement. The altitude of each probe was determined from the differential Ashtech GPS measurement and the INS attitude measurement.

$$h_j = 3.281 \cdot HI - (x_b - x_j) \sin \theta_{93} + (y_b - y_j) \cos \theta_{93} \sin \phi_{93} + (z_b - z_j) \cos \theta_{93} \cos \phi_{93} \quad (\text{ft})$$

$$j = l, n, r$$
(A11)

The reference static pressure was computed from:

$$Ps_{ref,j} = Ps_{grnd} - g \cdot \rho_{mid,j} (h_j - h_{grnd}) / 144 \quad (\text{psi})$$

$$j = l, n, r$$
(A12)

The density at the mid-altitude point was computed as:

$$\rho_{mid,j} = \rho_{grnd} + \frac{1}{2} (h_j - h_{grnd}) \frac{d\rho}{dh} \quad (\text{slugs/ft}^3)$$

$$j = l, n, r$$
(A13)

with $\frac{d\rho}{dh} = -6.8 \times 10^{-7} \text{ slugs/ft}^4$ (standard density lapse rate). The air density at the ground was corrected for non-standard conditions through:

$$\rho_{grnd} = \frac{144 \cdot Ps_{grnd}}{R \cdot T_{grnd}} \quad (\text{slugs/ft}^3)$$
(A14)

with $R = 1716.5 \frac{\text{ft lb}}{\text{slug } ^\circ \text{R}}$.

Compute Position Error Correction

The position error correction was determined via a least squares linear-fit of the difference between the probe and reference static pressures as a function of the probe dynamic pressure.

Probe Static and Dynamic Pressure Calculation

The probe static and dynamic pressures were corrected for local flow angularity based on wind tunnel derived calibration coefficients. The static and dynamic pressure coefficients are defined as:

$$C_S = \frac{Ps_{ref} - Ps_{probe}}{q_{ref}} \quad (\text{A15})$$

and

$$C_q = \frac{q_{ref} - q_{probe}}{q_{ref}} \quad (A16)$$

The reference values (subscripted *ref*) were the wind tunnel “truth” measurements. For the wing tip mounted NACA probes the coefficients were determined via a two-dimensional table lookup as a function of the reference angle of attack and sideslip. Tables 3 and 4 list the C_S and C_q table lookup values. The corrected wing tip probe dynamic (q_c) and static (Ps_c) pressures were computed from equations 29 and 30, respectively. The nose boom 5-hole probe dynamic (q_5) and static (Ps_5) pressures were computed from equations 20 and 21, respectively.

The position-error pressure correction was computed as the difference between the calibrated probe measurement and the reference value.

$$\Delta Pq_j = Ps_{c,j} - Ps_{ref,j} \quad (\text{psi})$$

$$j = l, r \quad (A17)$$

$$\Delta Pq_n = Ps_5 - Ps_{ref,n} \quad (A18)$$

Figures A5, A6, and A7 show the position error values of the nose, left and right boom probes, respectively, as a function of the probe calibrated dynamic pressure for the zero sideslip passes of both flights. Also shown on the figures is the least squares linear fit to the data. The linear fit coefficients were used as the position error correction coefficients for zero sideslip.

The effect of sideslip on the position error was determined by subtracting the zero sideslip position correction from the position error values at nonzero sideslip.

$$\Delta Pq_\beta = \Delta Pq_{(\beta \neq 0)} - \Delta Pq_{Fit(\beta=0)} \quad (A19)$$

Figures A8, A9, and A10 show the position error values due to sideslip of the nose, left and right boom probes, respectively. Also shown on the figures is the least squares linear fit to the data. The linear fit coefficients were used as the position error correction coefficients for non-zero sideslip. For the nose boom probe the effect of sideslip was symmetric about zero sideslip. For the wing tip probes the linear fit varied for positive and negative sideslip angles. The left and right boom corrections were nearly mirror images of each other. Figure A11 shows the two data sets combined with the left being the opposite sign as the right. The linear fit of the combined data sets was used for the tip boom correction coefficients.

The position error correction is applied to the static and dynamic pressure measurements through equations 36 through 39.

Angle of Attack Calibration

The angle of attack calibration was determined via a least squares linear fit of the measured value as a function of the reference value obtained from equation A8. The nose boom measured angle of attack was determined from equation 18. The wing tip values were obtained from the balsa vane measurements.

The airplane angular rates were assumed to be negligible. The data and linear fits are shown in figures A12, A13, and A14 for the nose, left and right booms, respectively. There was an apparent offset in the wing tip angle of attack measurements between flights 613 and 614. This was presumably due to a slight warping of the balsa vane with variation in temperature and humidity. Due to this offset the slope of the right and left boom calibration was computed from flight 613 values only. Flight 613 had a larger variation in the range of angles than Flight 614. The wing tip offset values for flight 614 were then computed using the slope calculations from flight 613.

Sideslip Angle Calibration

The sideslip calibration was determined in a similar manner as the angle of attack calibration. The reference sideslip value was obtained from equation A9. The nose boom measured sideslip angle was determined from equation 19. Figure A15 shows the nose boom sideslip calibration. There was a slight unresolved offset in the nose boom measurements between flights 613 and 614. The slope of the nose boom calibration curve was determined from flight 614 data since the majority of the sideslip data was obtained on that flight.

Figures A16 and A17 show the flank angle data and calibration for the left and right boom, respectively.

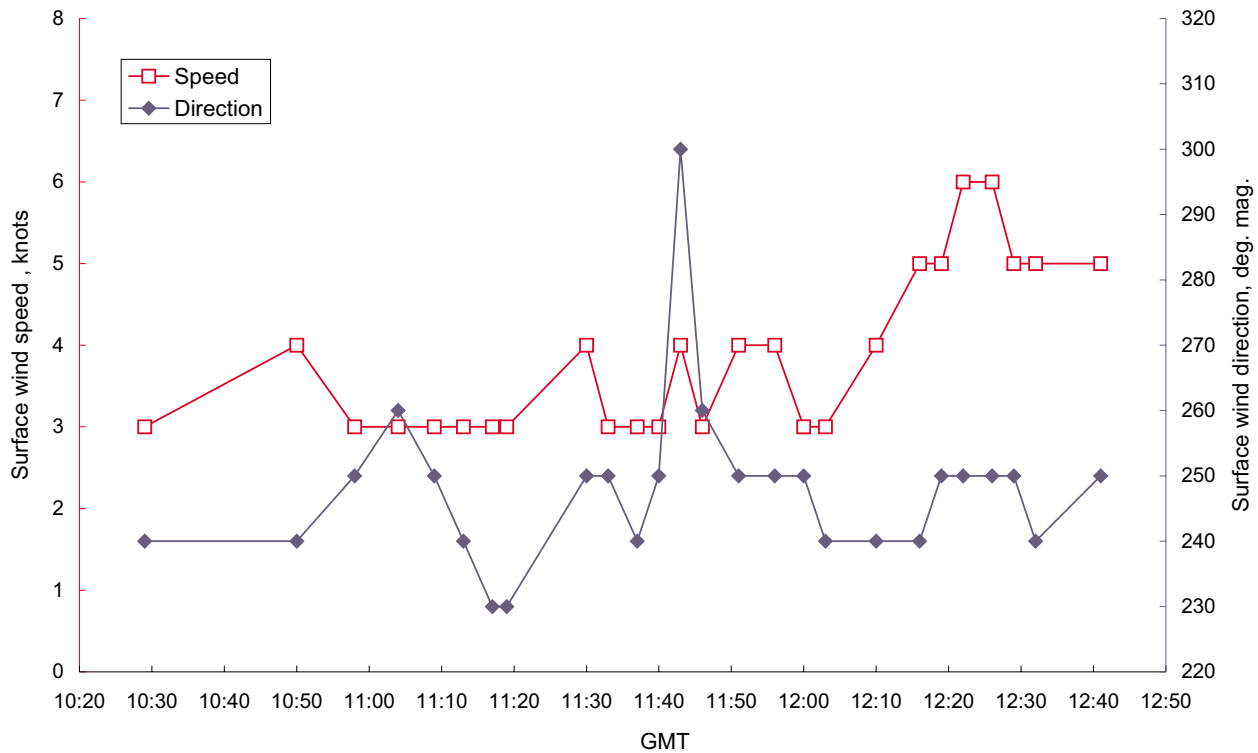


Figure A1(a). Surface wind history for Flight 613.

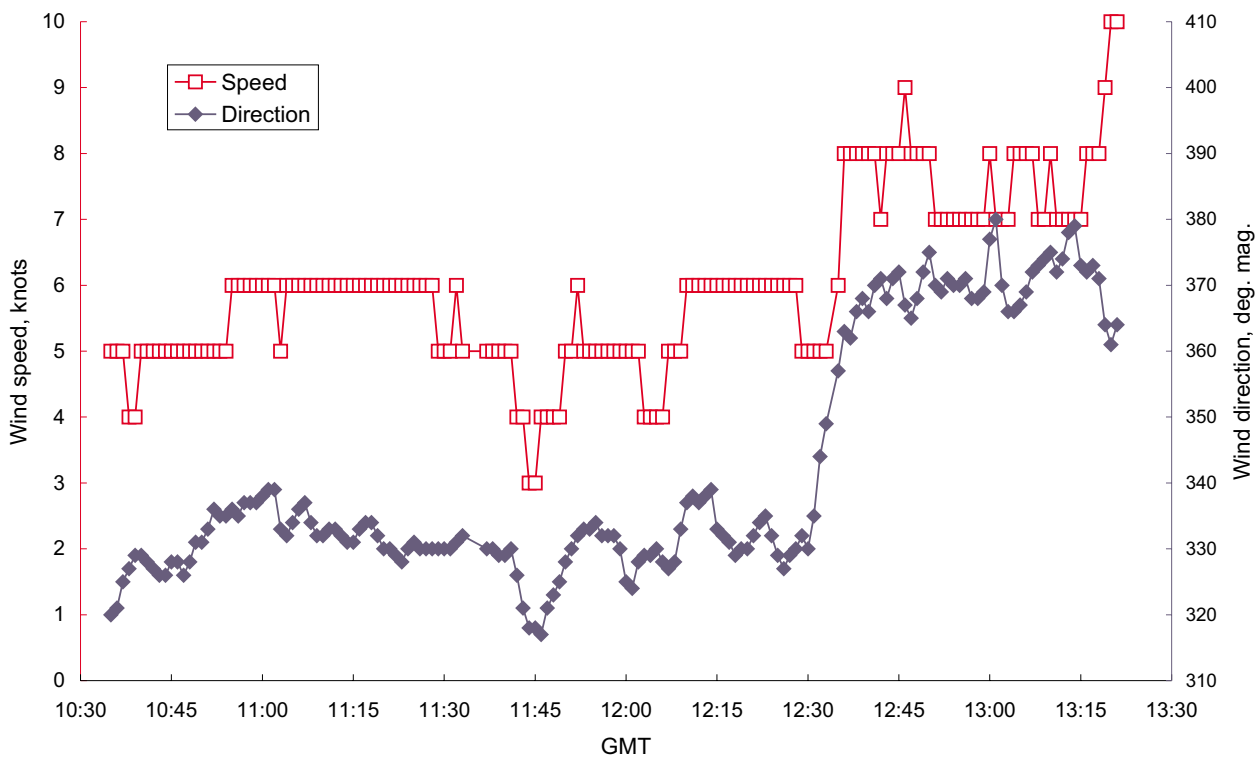


Figure A1(b). Surface wind history for Flight 614.

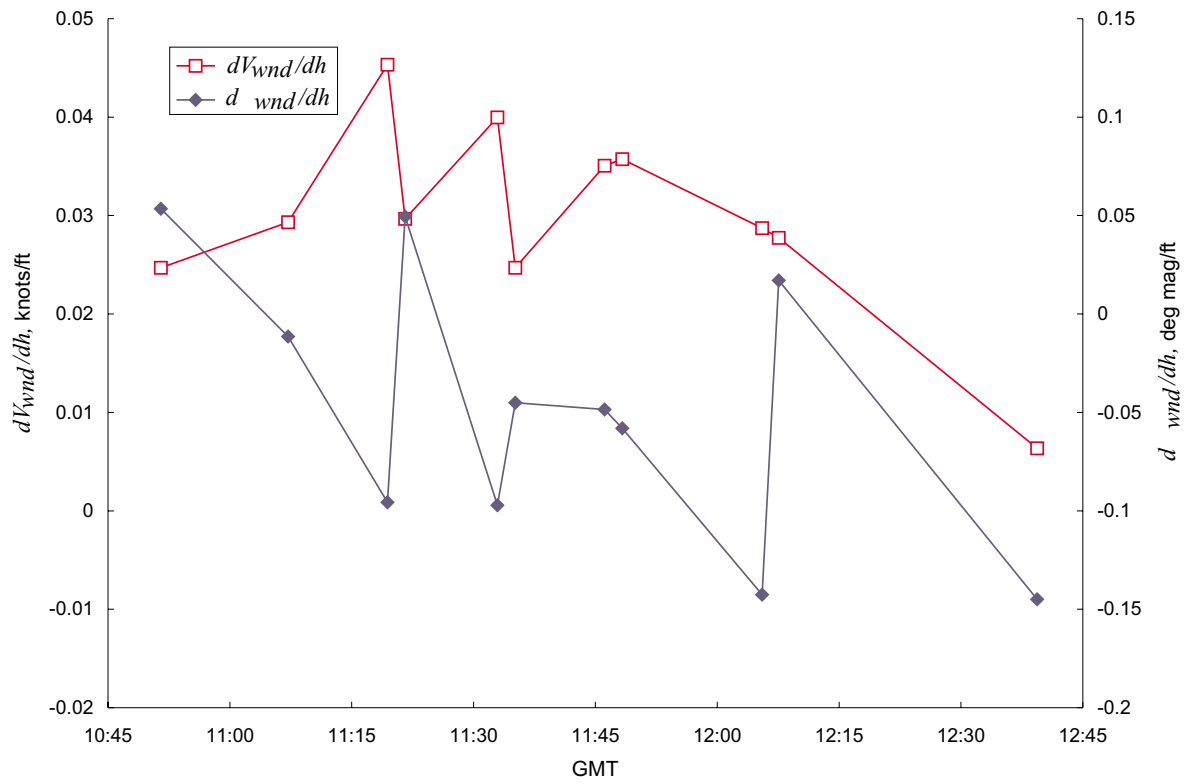


Figure A2(a). Wind laps rate history for Flight 613.

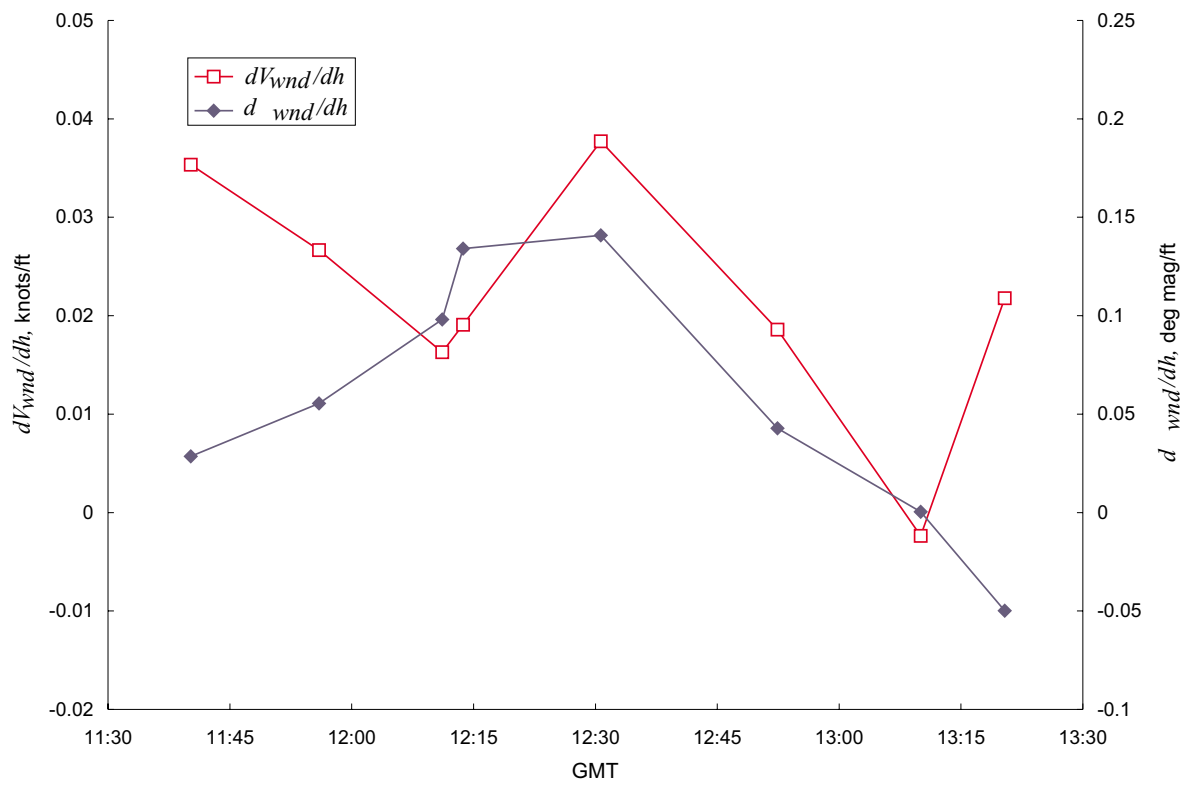


Figure A2(b). Wind laps rate history for Flight 614.

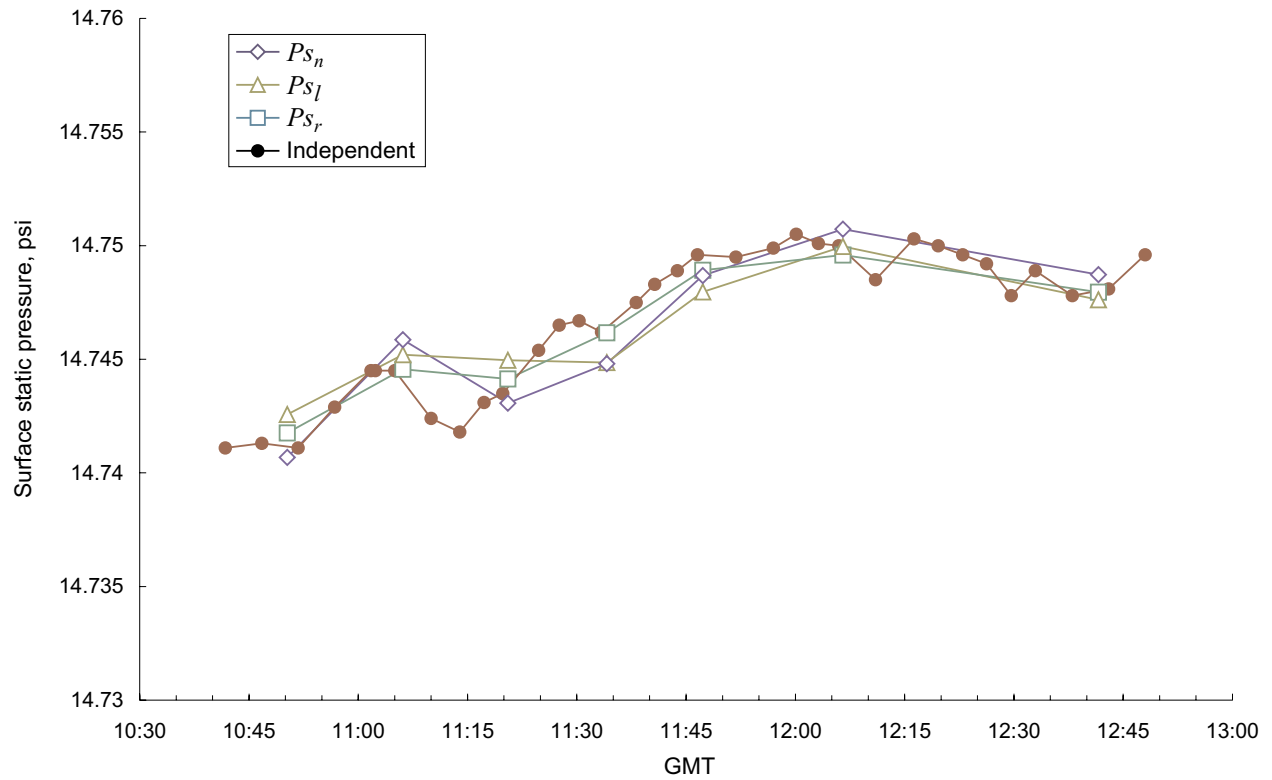


Figure A3(a). Ground static pressure history for Flight 613.

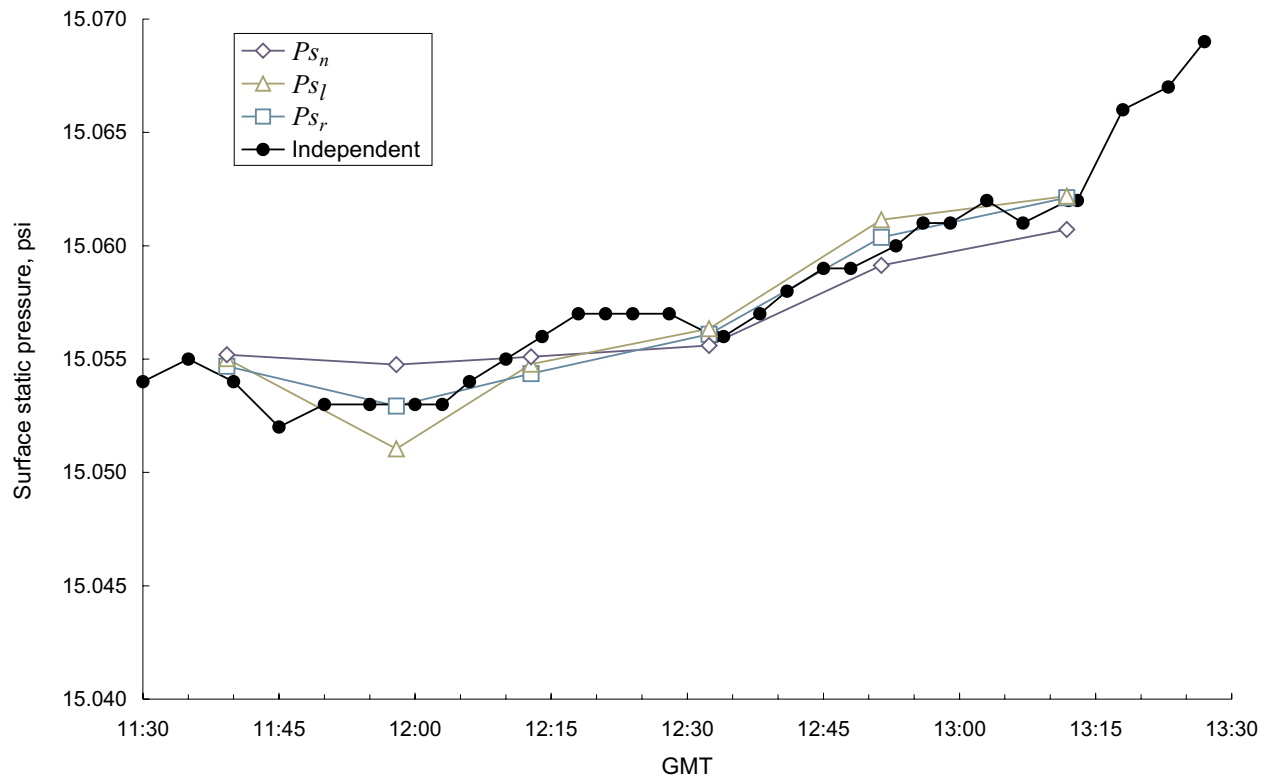


Figure A3(b). Ground static pressure history for Flight 614.

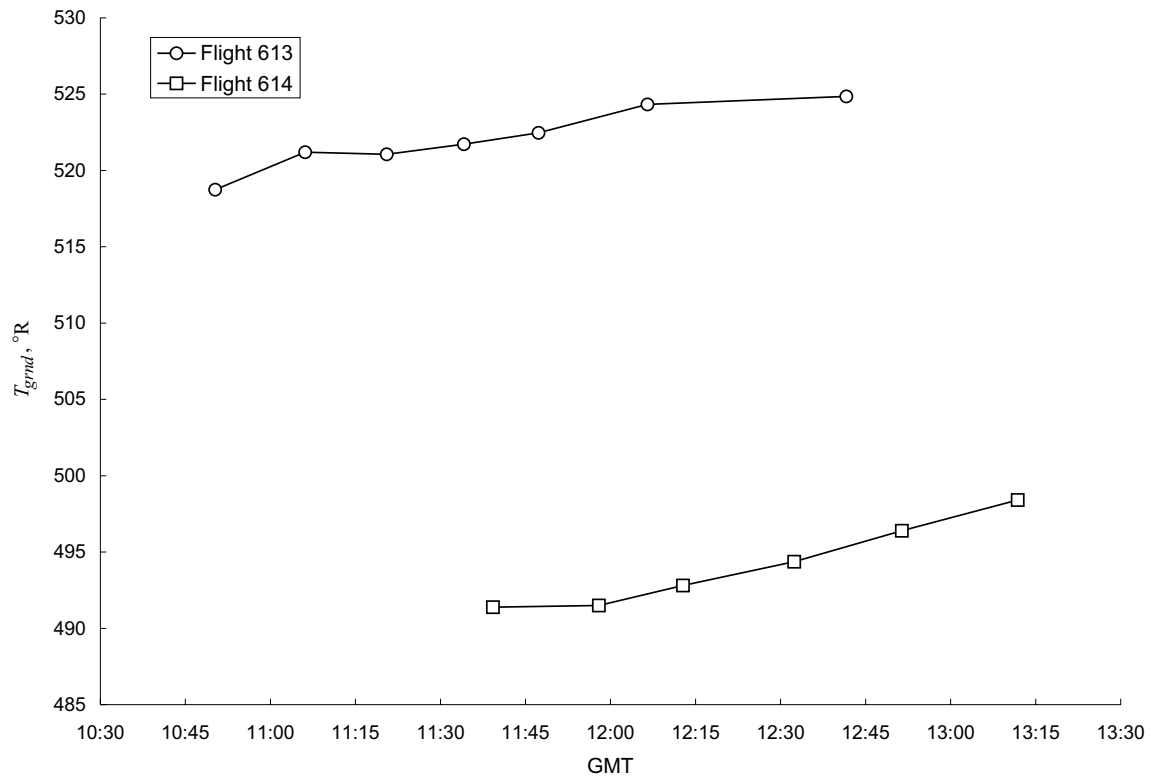


Figure A4. Ground temperature history for flights 613 and 614.

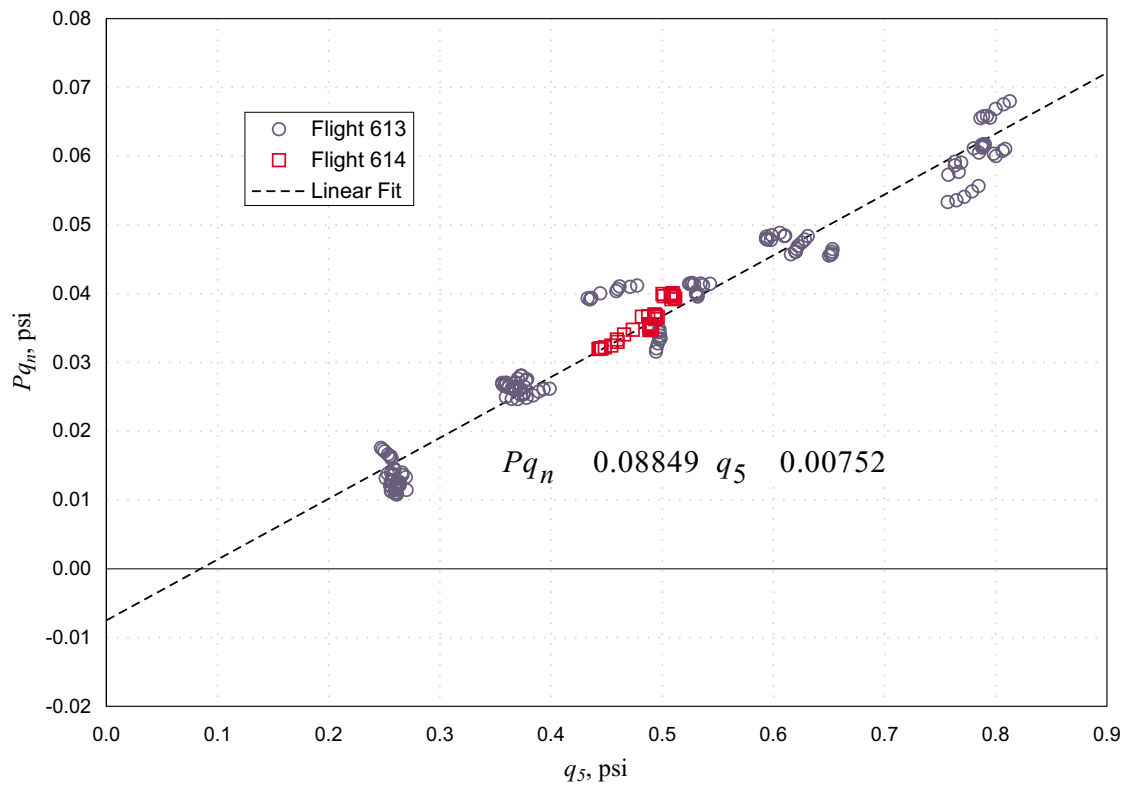


Figure A5. Nose boom 5-hole probe position error correction.

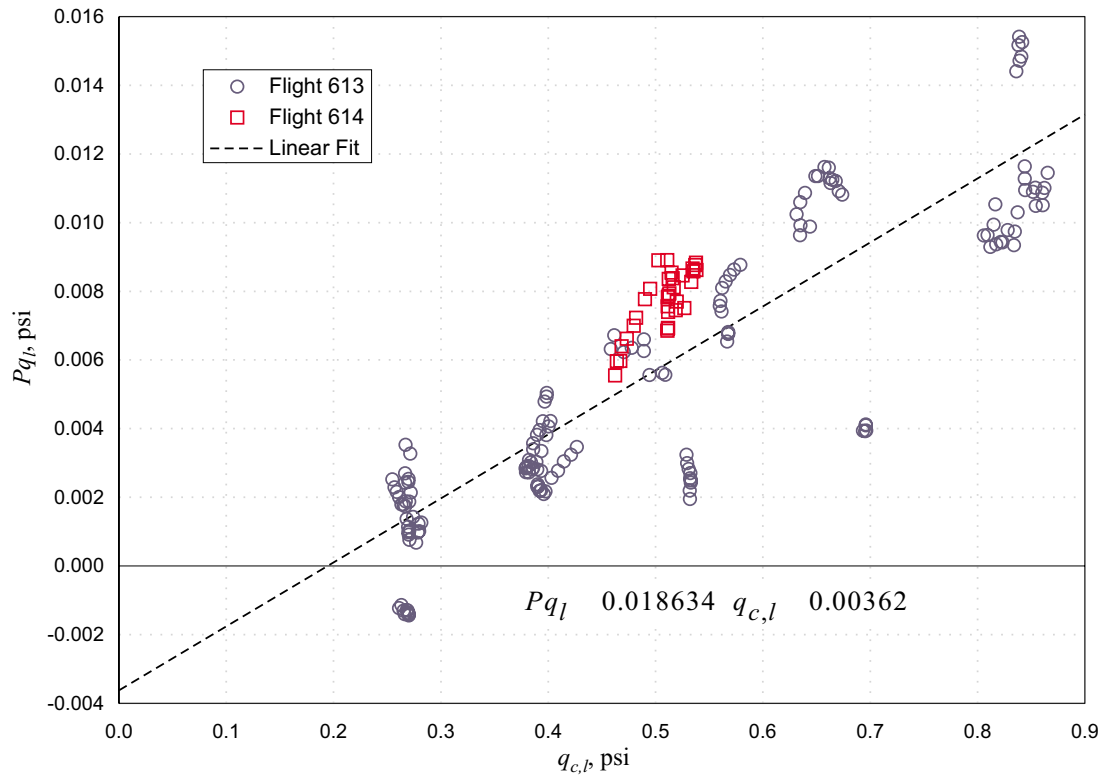


Figure A6. Left wing tip boom probe position error correction.

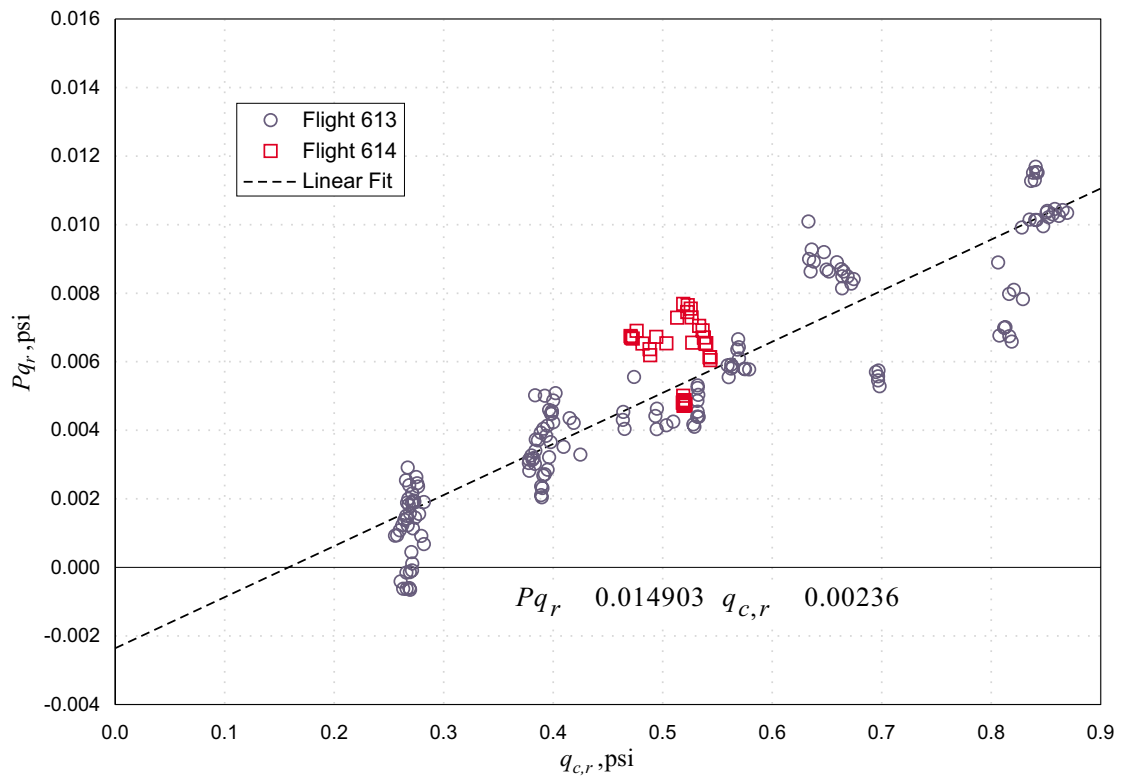


Figure A7. Right wing tip boom probe position error correction.

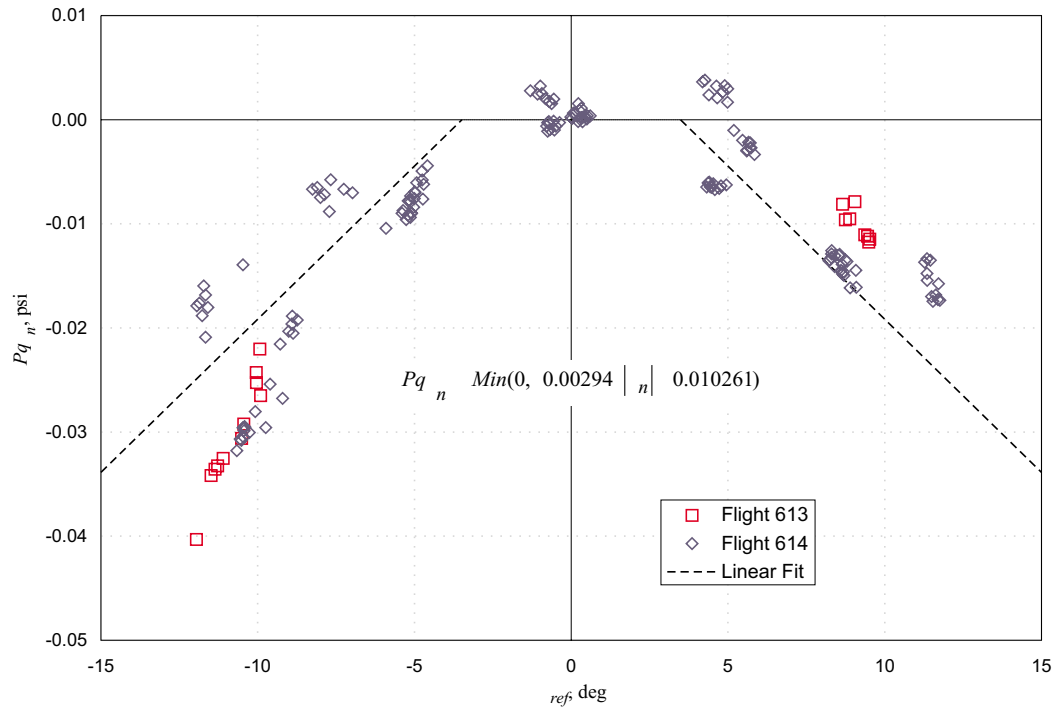


Figure A8. Nose boom probe position error correction with sideslip.

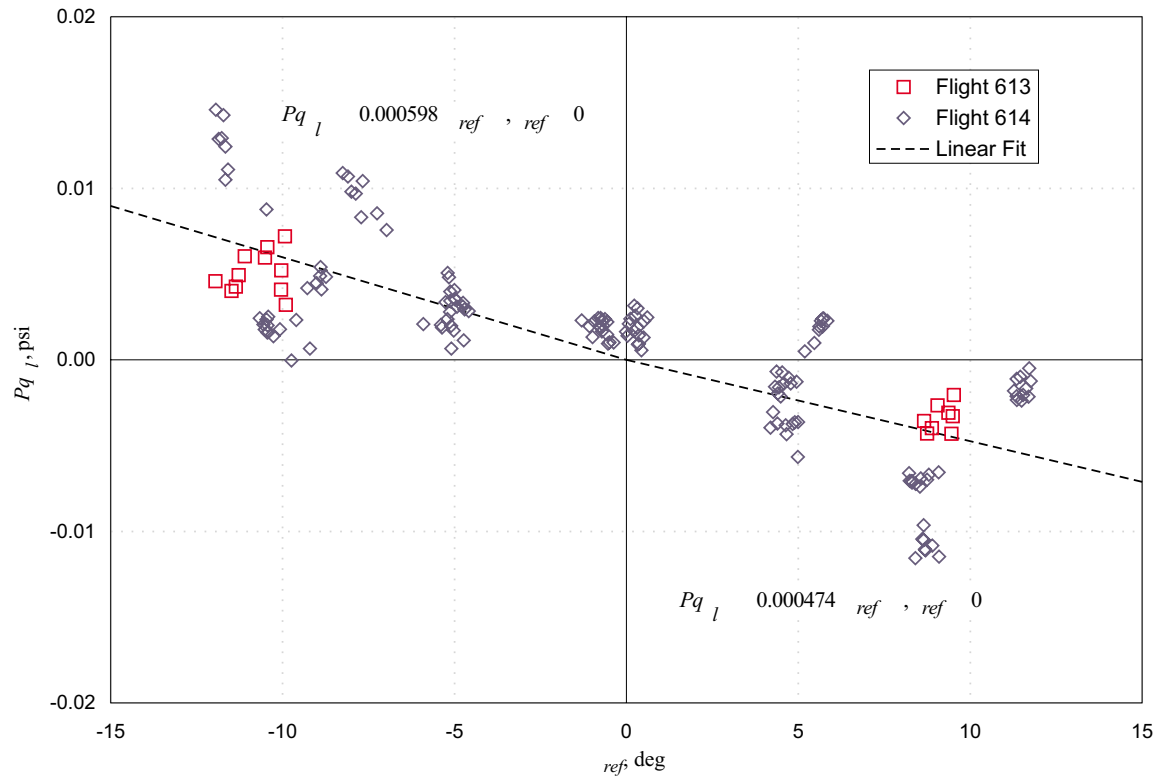


Figure A9. Left boom probe position error correction with sideslip.

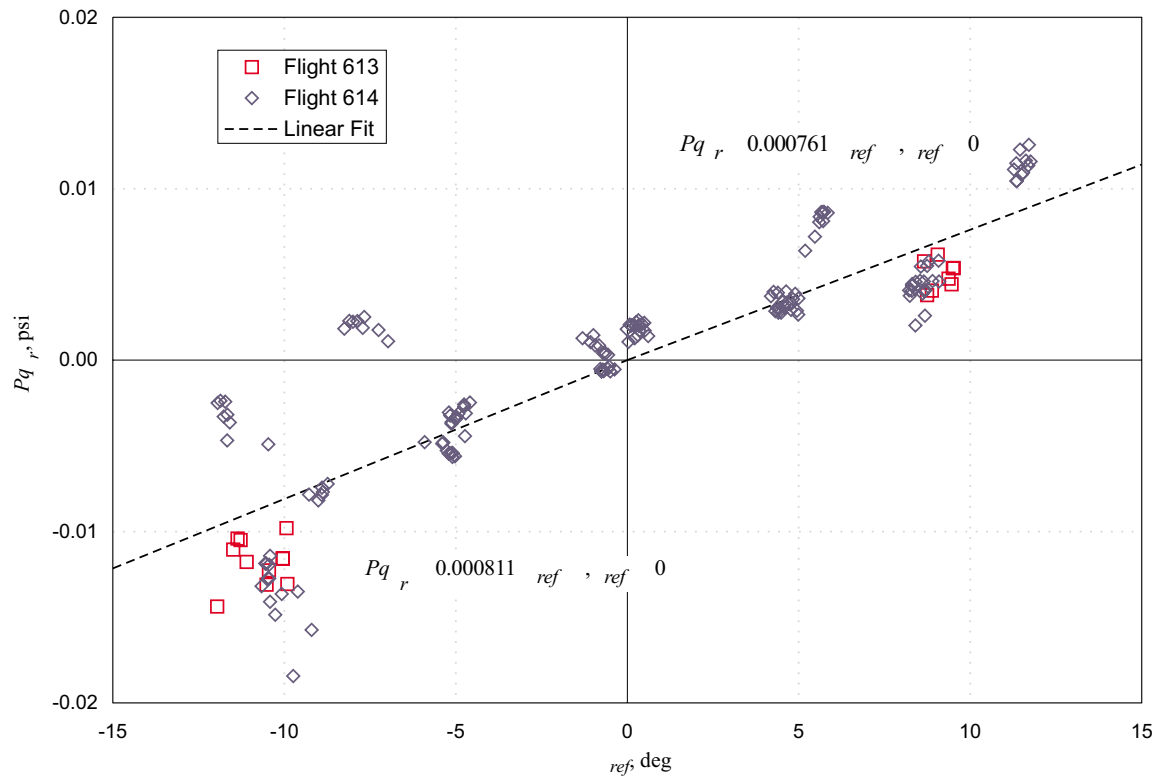


Figure A10. Right boom probe position error correction with sideslip.

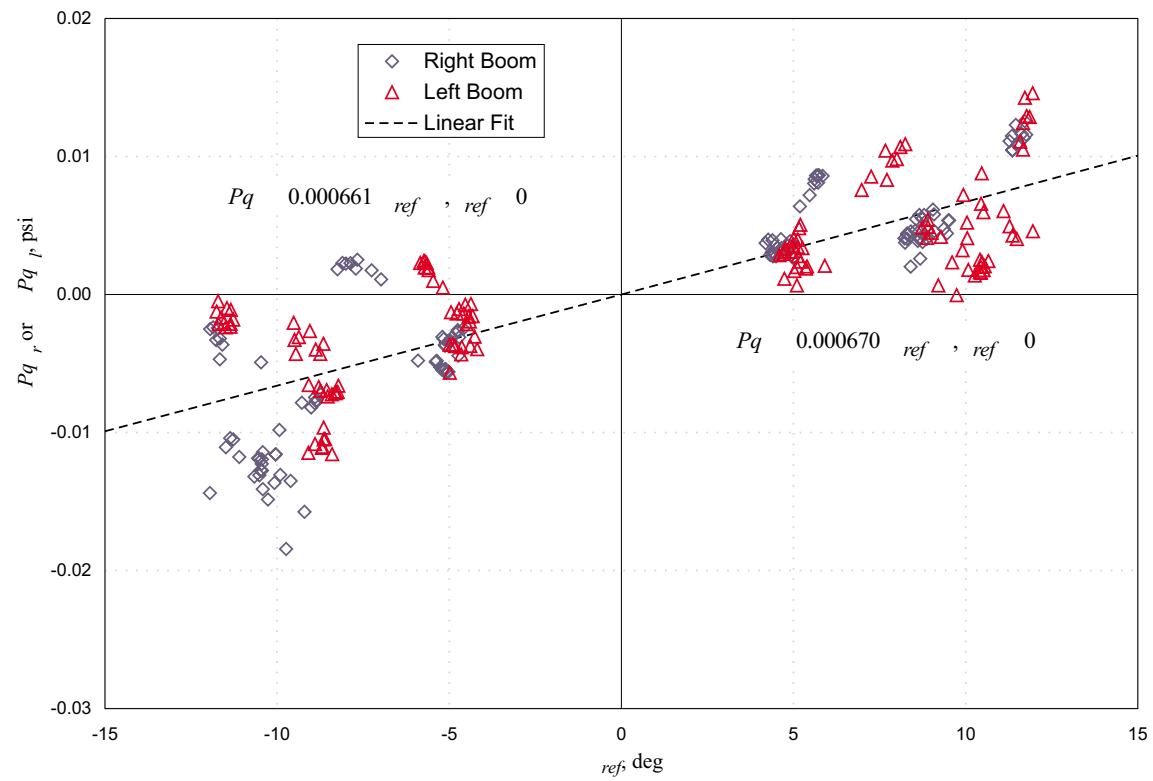


Figure A11. Combined right and left probe position error correction with sideslip.

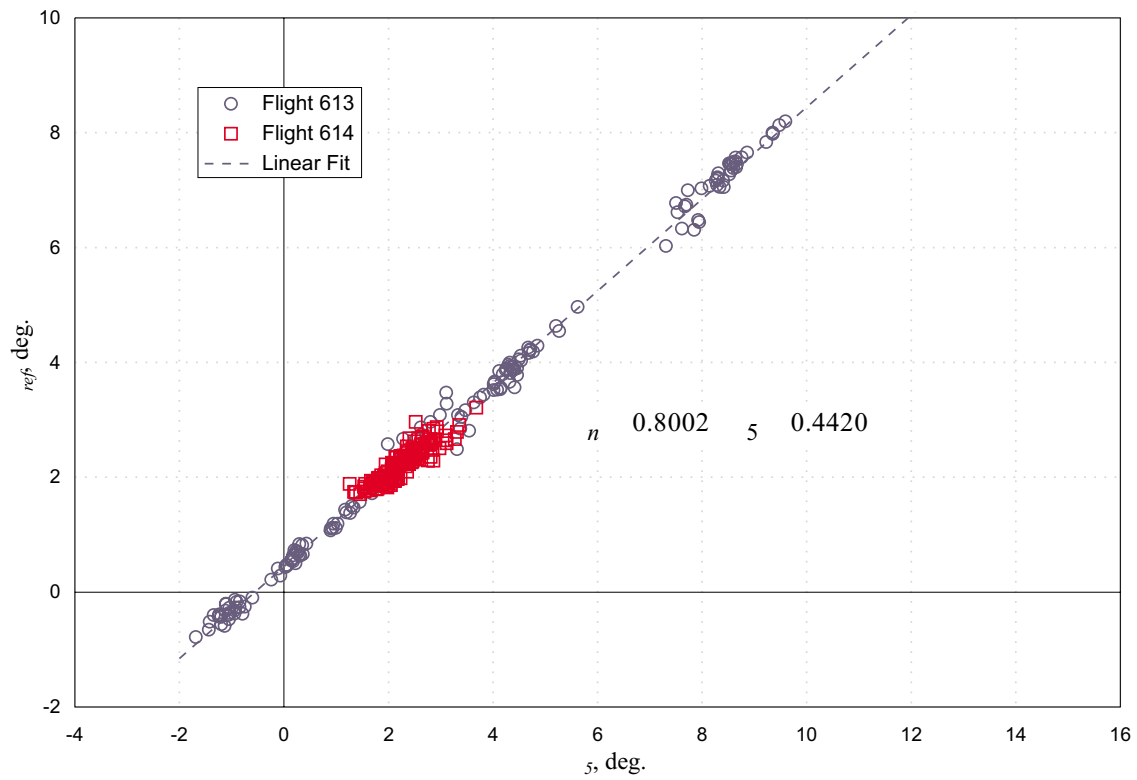


Figure A12. Nose boom angle of attack calibration.

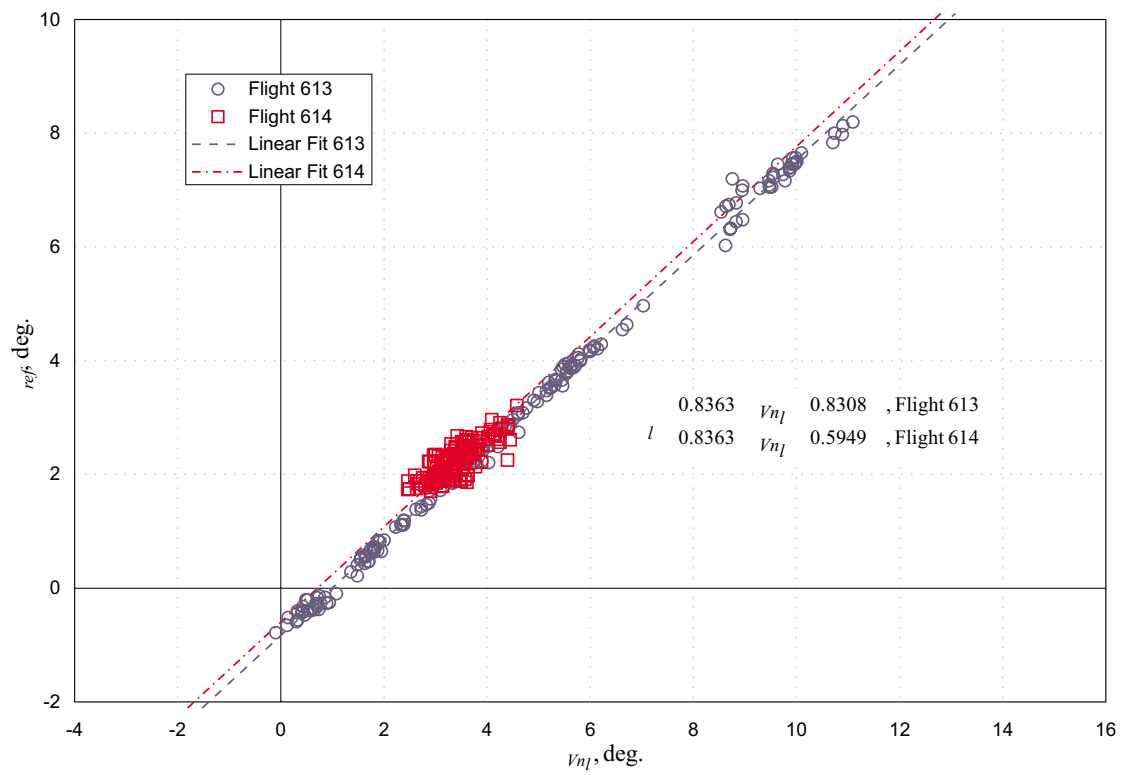


Figure A13. Left boom angle of attack calibration.

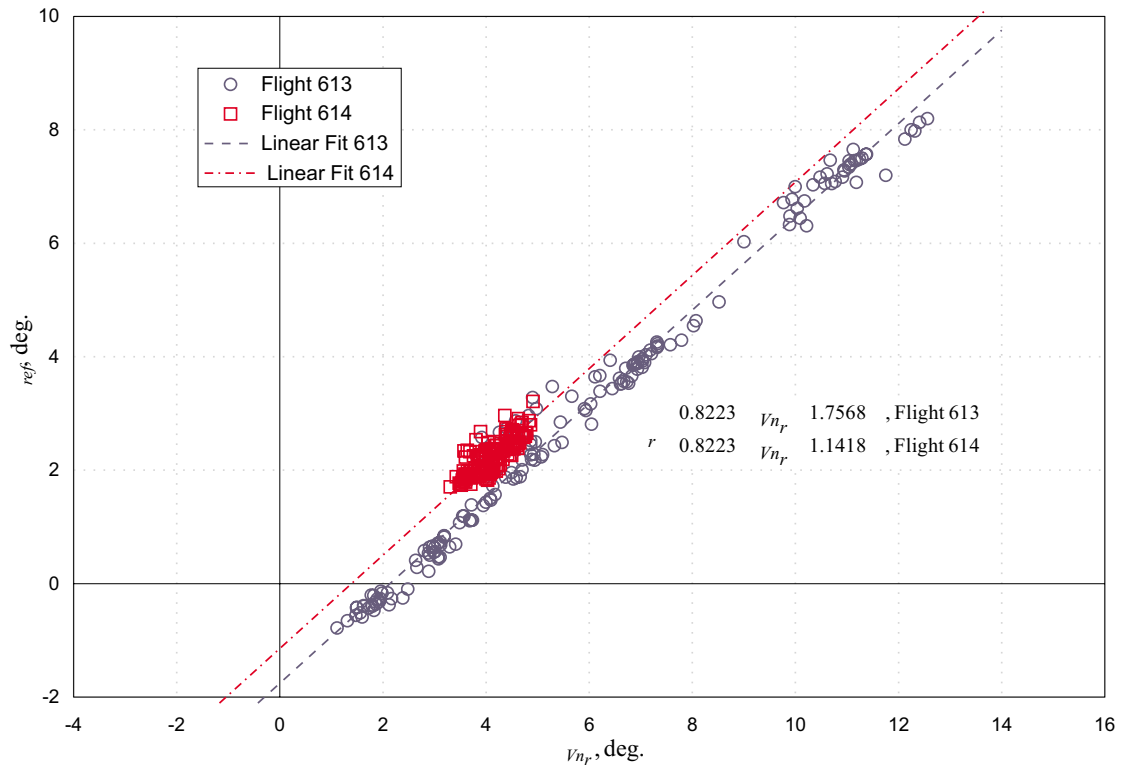


Figure A14. Right boom angle of attack calibration.

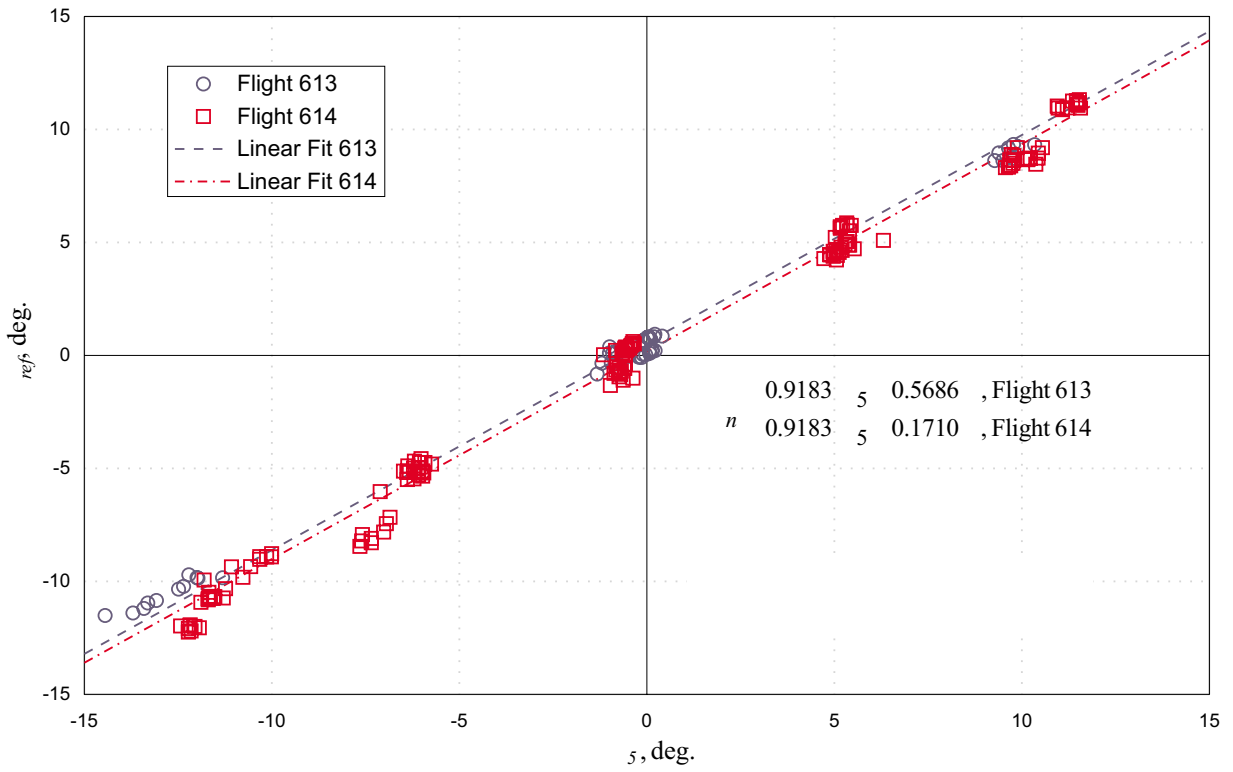


Figure A15. Nose boom sideslip calibration.

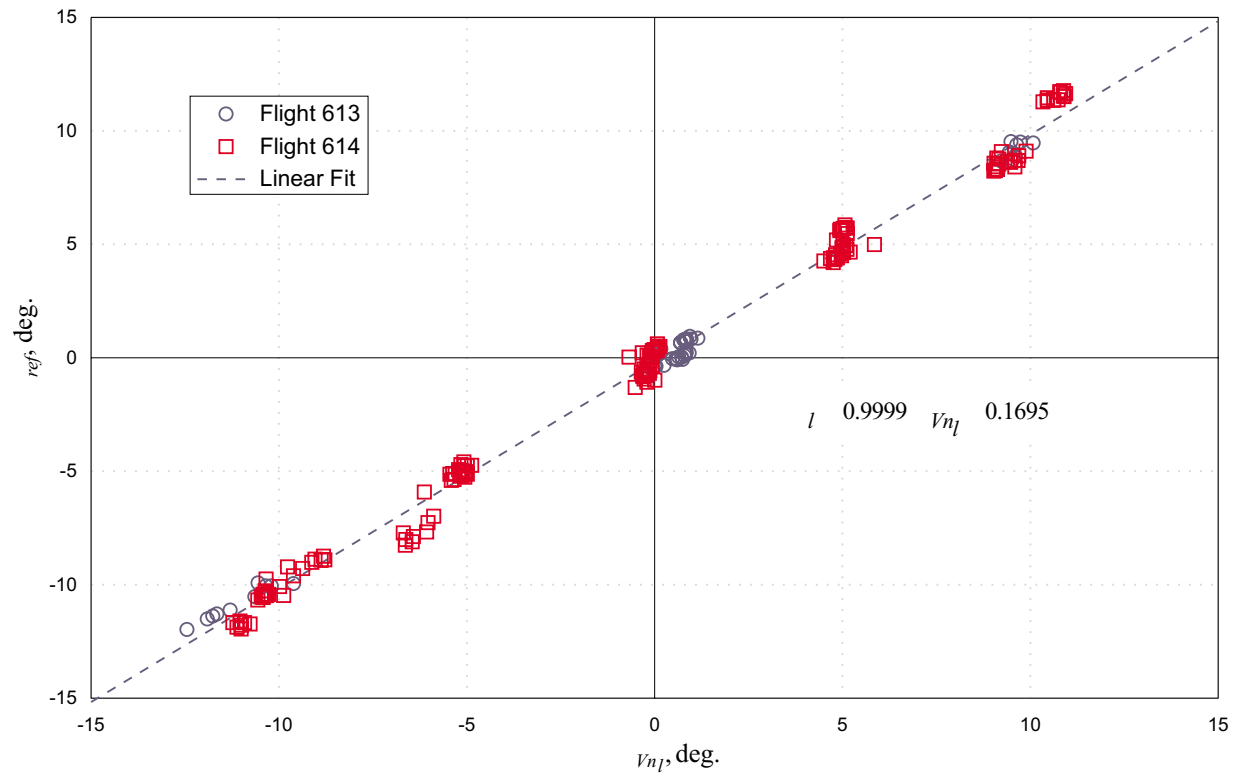


Figure A16. Left boom sideslip calibration.

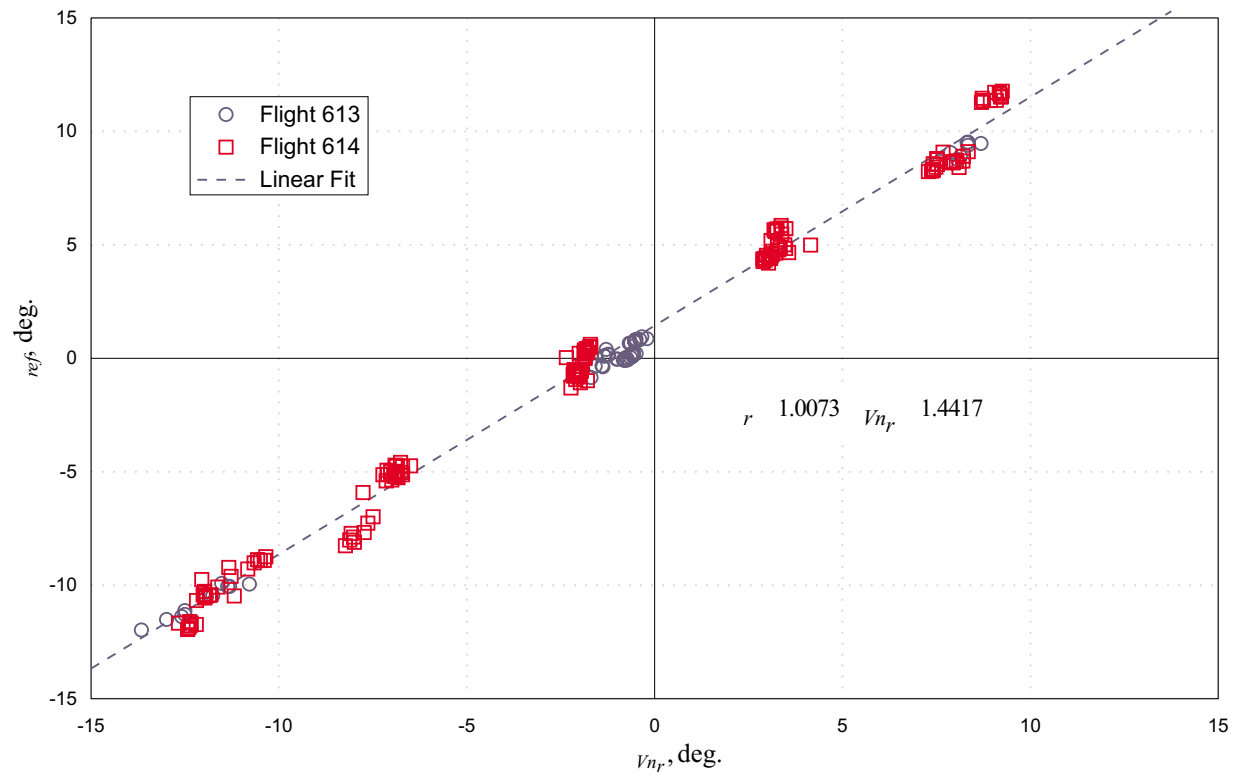


Figure A17. Right boom sideslip calibration.

| | | | | |
|--|---|--|--|--|
| REPORT DOCUMENTATION PAGE | | | Form Approved OMB No. 0704-0188 | |
| Public reporting burden for this collection of information is estimated to average 1 hour per response, including the time for reviewing instructions, searching existing data sources, gathering and maintaining the data needed, and completing and reviewing the collection of information. Send comments regarding this burden estimate or any other aspect of this collection of information, including suggestions for reducing this burden, to Washington Headquarters Services, Directorate for Information Operations and Reports, 1215 Jefferson Davis Highway, Suite 1204, Arlington, VA 22202-4302, and to the Office of Management and Budget, Paperwork Reduction Project (0704-0188), Washington, DC 20503. | | | | |
| 1. AGENCY USE ONLY (Leave blank) | | 2. REPORT DATE September 1999 | 3. REPORT TYPE AND DATES COVERED Technical Memorandum | |
| 4. TITLE AND SUBTITLE Flight Data Reduction of Wake Velocity Measurements Using an Instrumented OV-10 Airplane | | | 5. FUNDING NUMBERS WU 538-04-11-12 | |
| 6. AUTHOR(S) Dan D. Vicroy, Robert A. Stuever, Eric C. Stewart, and Robert A. Rivers | | | | |
| 7. PERFORMING ORGANIZATION NAME(S) AND ADDRESS(ES) NASA Langley Research Center Hampton, VA 23681-2199 | | | 8. PERFORMING ORGANIZATION REPORT NUMBER L-17892 | |
| 9. SPONSORING/MONITORING AGENCY NAME(S) AND ADDRESS(ES) National Aeronautics and Space Administration Washington, DC 20546-0001 | | | 10. SPONSORING/MONITORING AGENCY REPORT NUMBER NASA/TM-1999-209552 | |
| 11. SUPPLEMENTARY NOTES | | | | |
| 12a. DISTRIBUTION/AVAILABILITY STATEMENT Unclassified-Unlimited Subject Category 03 Distribution: Nonstandard Availability: NASA CASI (301) 621-0390 | | | 12b. DISTRIBUTION CODE | |
| 13. ABSTRACT (Maximum 200 words) A series of flight tests to measure the wake of a Lockheed C-130 airplane and the accompanying atmospheric state have been conducted. A specially instrumented North American Rockwell OV-10 airplane was used to measure the wake and atmospheric conditions. An integrated database has been compiled for wake characterization and validation of wake vortex computational models. This paper describes the wake-measurement flight-data reduction process. | | | | |
| 14. SUBJECT TERMS Wake Vortex, Flight Test, Wake Encounters, Data Reduction | | | 15. NUMBER OF PAGES 66 | |
| | | | 16. PRICE CODE A04 | |
| 17. SECURITY CLASSIFICATION OF REPORT Unclassified | 18. SECURITY CLASSIFICATION OF THIS PAGE Unclassified | 19. SECURITY CLASSIFICATION OF ABSTRACT Unclassified | 20. LIMITATION OF ABSTRACT UL | |